Virus Research 355 (2025) 199561

Contents lists available at ScienceDirect

Virus Research

journal homepage: www.elsevier.com/locate/virusres

Regulation of inflammatory cytokines and activation of PI3K/Akt pathway by Yiqi Jiedu Formula in recurrent Herpes Simplex Keratitis: Experimental and network pharmacology evidence

Shuyu Xiao [a], Wanhong Miao [a], Leilei Wang [b], Lei Wang [b], Sisi Tang [c], Huihui Xu [d], Ying Yu [a,*]

[a] Department of Ophthalmology, Shuguang Hospital Affiliated to Shanghai University of Traditional Chinese Medicine, No.185 Pu'an Road, Huangpu District, Shuguang, Shanghai 201203, China
[b] Department of Ophthalmology, Shanghai Eye Disease Control Center, Shuguang, 200041, China
[c] Department of Ophthalmology, Shanghai Songjiang District Fangta Traditional Chinese Medicine Hospital, Shuguang, 201699, China
[d] Department of Ophthalmology, Shanghai Aier Songchen Eye Hospital, Shuguang, 201699, China

ARTICLE INFO

Keywords:
Herpes Simplex Keratitis
Network pharmacology
Molecular docking
Akt signaling pathway
Interleukin-4

ABSTRACT

Objective: This study investigates the therapeutic effects of the Yiqi Jiedu (YQJD) formula on Herpes Simplex Keratitis (HSK) induced by herpes simplex virus type 1 (HSV-1) and elucidates its mechanisms of action through experimental and network pharmacology approaches.
Methods: Active ingredients of the YQJD formula were identified using UPLC-HRMS. Network pharmacology was employed to predict shared targets between YQJD and HSK, focusing on the PI3K/Akt signaling pathway. Molecular docking was performed to assess the interaction between key ingredients and targets. *In vivo*, an HSK mouse model was used to evaluate the YQJD formula's impact on corneal lesions and inflammatory factors. *In vitro*, human corneal epithelial cells (HCECs) were infected with HSV-1 to assess the formula's effect on IL-4 expression.
Results: UPLC-HRMS identified 34 compounds in YQJD, with Isovitexin and Formononetin exhibiting high oral bioavailability. Network analysis revealed 97 intersecting targets, implicating the PI3K/Akt pathway in YQJD's mechanism. Molecular docking showed strong affinities between IL-4, IL-6, and YQJD compounds. *In vivo*, YQJD significantly improved corneal lesions and modulated the expression of IL-4, IL-6, and AKT. *In vitro*, YQJD-containing serum regulated IL-4 expression in HCECs post-HSV-1 infection.
Conclusion: The YQJD formula ameliorates Herpes Simplex Keratitis by regulating inflammatory cytokines and activating the PI3K/Akt pathway, offering a potential therapeutic strategy for HSK.

1. Introduction

Herpes simplex virus type 1 (HSV-1) infection is one of the most common infectious diseases worldwide, characterized by significant viral transmissibility and recurrence (Van Wagoner et al., 2023; Johnston et al., 2022; Rathbun and Szpara, 2021). HSV-1 primarily infects the oral mucosa and eyes, leading to clinical symptoms such as oral herpes and keratitis (Hinojosa and Ammari, 2023; Danastas et al., 2023; Naqvi et al., 2024). Herpes Simplex Keratitis (HSK) is a severe eye disease that can result in corneal opacity, vision impairment, and even blindness (Almeida et al., 2022; Sendra et al., 2021). Although traditional antiviral drugs are widely used clinically, their side effects and the increasing viral resistance make exploring new treatment strategies more urgent (Feld et al., 2023; McCarthy, 2022).

Yiqi Jiedu Formula (YQJD) is a complex herbal preparation traditionally used to enhance immunity, detoxify, and regulate Yin-Yang balance (Lu et al., 2023; Zhou et al., 2024). Recent clinical and experimental studies have demonstrated its efficacy in treating various inflammatory and infectious diseases (Zhou et al., 2024) and revealed its immunomodulatory and anti-inflammatory effects at the molecular level (Zhou et al., 2024; Yin et al., 2024). However, the specific mechanisms of action in combating HSV-1 infection and the resulting keratitis are not entirely clear. It is known that inflammatory factors such as interleukin-4 (IL-4) and interleukin-6 (IL-6) play crucial roles in the inflammatory response triggered by HSV-1 (Oh et al., 2023; Jaggi et al., 2022). These cytokines regulate the host's immune response and

* Corresponding author.
E-mail address: loyis81@163.com (Y. Yu).

https://doi.org/10.1016/j.virusres.2025.199561
Received 7 January 2025; Received in revised form 11 March 2025; Accepted 20 March 2025
Available online 20 March 2025

influence the pathological progression after viral infection by activating or inhibiting specific cellular signaling pathways (Mustafa et al., 2022). Research on these pathways not only contributes to understanding the pathogenesis of Herpes Simplex Keratitis but also provides valuable clues for exploring the therapeutic potential of the YQJD Formula (Li Puma et al., 2023; Haghighi-Najafabadi et al., 2021; Jiang et al., 2022).

The Phosphoinositide 3-kinase (PI3K)/Akt signaling pathway is one of the crucial pathways that regulate cell survival, proliferation, migration, and apoptosis, and its activation state is essential for maintaining normal cell function (Qu et al., 2021; Barzegar Behrooz et al., 2022; Du et al., 2022). In viral infections, especially HSV-1 infection, activating the PI3K/Akt signaling pathway is particularly critical. This pathway regulates the host cell's survival mechanisms and affects the virus's lifecycle, including replication and assembly processes (Li et al., 2020). Additionally, the activation or inhibition of the PI3K/Akt pathway directly impacts the extent of the inflammatory response by regulating the expression of downstream inflammatory factors and the release of cytokines, playing a significant role in Herpes Simplex Keratitis (Chou et al., 2021, Hu et al., 2021, Efferth and Oesch, 2021).

Preliminary studies suggest that YQJD may exert its antiviral and anti-inflammatory effects by directly or indirectly influencing the activity of the PI3K/Akt signaling pathway (Zhou et al., 2024). The YQJD formula contains various natural medicinal components, such as certain herbal extracts, which may potentially regulate the PI3K/Akt pathway. This regulatory effect may involve targeting key proteins in the pathway, such as PI3K, Akt, and downstream NF-κB (Zhang et al., 2022; Xiao et al., 2022). By inhibiting or promoting the activity of these key proteins, the YQJD formula can alleviate virus-induced cell damage, modulate the intensity of inflammatory responses, and affect the virus's replicative capability.

To systematically explore the role and mechanism of the YQJD in treating HSK, this study first employed ultra-performance liquid chromatography-high resolution mass spectrometry (UPLC-HRMS) to identify its active compounds. Bioinformatics analysis, including Gene Ontology (GO) and Kyoto Encyclopedia of Genes and Genomes (KEGG) pathway enrichment via the DAVID database, was conducted to elucidate the molecular mechanisms of YQJD. Molecular docking was then performed to verify the interactions between YQJD's active compounds and key inflammatory factors IL-4 and IL-6, predicting potential binding sites and affinities to provide insights into its anti-inflammatory mechanisms. An HSK animal and cell model was also established to evaluate YQJD's effects on inflammation following viral infection and its potential clinical applications. This study provides a theoretical and experimental basis for developing novel anti-HSV-1 drugs and therapeutic strategies.

In summary, this study demonstrates that YQJD alleviates HSV-1-induced HSK inflammation by modulating IL-4 and IL-6 levels and activating the PI3K/Akt signaling pathway. These findings enhance our understanding of YQJD's therapeutic effects on HSK and highlight traditional Chinese medicine's clinical and scientific significance in antiviral and anti-inflammatory therapy, laying the groundwork for novel anti-HSV-1 treatments.

2. Materials and methods

2.1. Determination of components in YQJD formula by UPLC-HRMS

The YQJD formula is composed of Huang Qi (Astragalus mongholicus Bunge.), Bai Zhu (Atractylodes macrocephala Koidz.), Fang Feng [Saposhnikovia divaricata (Turcz. ex Ledeb.) Schischk.], Jin Yin Hua (Lonicera japonica Thunb.), Pu Gong Ying (Taraxacum mongolicum Hand.-Mazz.), Da Qing Ye (Isatis tinctoria subsp. Tinctoria.), Zi Cao [Arnebia euchroma (Royle ex Benth.) I.M.Johnst.], Chan Tui (Cryptotympana pustulata Fabricius.), Fu Ling {Wolfiporia extensa (Peck) Ginns [syn. Poria cocos (Schw.)]}, Sheng Di Huang [Rehmannia glutinosa (Gaertn.) DC.] and Chai Hu (Bupleurum chinense DC.). The preparation process of the YQJD formula mass spectrometry solution is as follows: firstly, accurately measure 1 mL of the YQJD formula solution and transfer it to a 10 mL volumetric flask, dilute it with deionized water. Subsequently, centrifuge at 12,000 rpm for 5 min and filter the supernatant through a 0.22 μm microporous membrane for subsequent analysis. In the chromatographic analysis, a Waters ACQUITY UPLC® HSS T3 column (specification: 2.1×100.0 mm, particle size 1.8 μm) was utilized, maintaining the column temperature at 30 °C. Mobile phase A consisted of a water solution containing 0.1 % formic acid, with an injection volume of 3 μL, and the autosampler temperature set at 4 °C. Mobile phase B was acetonitrile, and gradient elution was performed as shown in Table S1. Mass spectrometry was detected using an electrospray ionization (ESI) source in both negative and positive ion modes, with specific parameters detailed in Table S2.

The composition of the YQJD formula was analyzed using UPLC-HRMS technology. We referenced the mass spectrometry information from the natural product HR-MS/MS spectral library 1.0.1 and comprehensively analyzed the UPLC-Q-TOF/MS system. This system combines the rapid separation capabilities of UPLC with the high-sensitivity detection features of high-resolution tandem mass spectrometry (HR-MS/MS). Initial screening was based on each chromatographic peak's mass spectrometry information, followed by compound confirmation by matching each peak's exact mass and fragment information. Additionally, the extracted compound information was compared and integrated with public databases to enhance the accuracy and reliability of identification.

2.2. Research in network pharmacology

2.2.1. Active ingredients and targets analysis of YQJD formula

The active ingredients and targets of the YQJD formula were obtained through the TCM Systems Pharmacology Database and Analysis Platform (TCMSP) (http://lsp.nwu.edu.cn/tcmsp.php) and the Bioinformatics Annotation Database for the Molecular Mechanism of TCM (BATMAN-TCM) (http://bionet.ncpsb.org.cn/batman-tcm/). We used absorption, distribution, metabolism, and excretion (ADME) parameters, specifically focusing on oral bioavailability (OB) and drug-likeness (DL) as key indicators to screen compounds and targets. In particular, compounds and targets were considered to have potential biological activity when OB $\geq$ 30 % and DL $\geq$ 0.18.

2.2.2. Key target analysis of YQJD formula in the treatment of HSK

In the current study, data on relevant targets of HSK, as well as resistance and toxicity in prophylactic treatment with acyclovir, are relatively limited (van Velzen et al., 2013). Recurrence of HSK often accompanies more severe corneal reactions, such as corneal opacity or scar formation. By comprehensively utilizing the key terms "Herpes Simplex Keratitis," "corneal opacity," "corneal scar," and "corneal injury (inflammation)," this study searched for disease targets related to HSK from GeneCards (https://www.genecards.org/) and OMIM (http://www.omim.org/) databases. The intersection of the targets of the YQJD formula and HSK was identified as the crucial target for treating HSK with the YQJD.

2.2.3. GO and KEGG enrichment analysis

The key targets of the YQJD formula in treating HSK were subjected to GO functional enrichment analysis and KEGG pathway enrichment analysis using the DAVID database (https://david.ncifcrf.gov/). The GO analysis included Biological Processes (BP), Molecular Functions (MF), and Cellular Components (CC). The identifier was set as "OFFICIAL_GENE_SYMBOL," the species as Homo sapiens, and a criterion of FDR $<$ 0.05 was applied for selection. Enrichment analysis based on the KEGG method was presented in bubble charts and tabular forms to highlight critical biological pathways and potential biological functions.

2.2.4. Protein-protein interaction (PPI) network construction

To delve into the mechanism of action of YQJD in treating HSK, key targets were imported into the STRING database (https://string-db.org/) to construct a PPI network. A confidence threshold of 0.7 was set to filter out highly reliable interaction relationships. This network revealed intricate interaction patterns among active components' targets, ensuring the analysis results' reliability and accuracy. Furthermore, in this study, downstream genes based on the PI3K/Akt signaling pathway were selected from the STING database, forming a PPI network with a comprehensive score ≥ 0.7, aiming to provide a more solid scientific basis for unraveling the multi-target molecular mechanisms of YQJD in treating HSK.

2.2.5. Constructing and analyzing multidimensional networks

This study established three multidimensional bioinformatics networks to investigate the interaction mechanisms among active compounds, diseases, and their targets. Using Cytoscape software (version 3.10.1), we generated a compound-target (C-T) association network, a target-disease (T-D) interaction network, and an integrated network of formula-compound-target-disease (F-C-T-D), followed by multidimensional visual analysis.

2.2.6. Molecular docking experiments

Molecular docking technology served as this study's core drug discovery and screening method. We utilized SWISS-MODEL software (https://swissmodel.expasy.org/interactive) to build three-dimensional protein models of NF-κB1, IL-4, and IL-6 to enhance screening accuracy. The chemical structures of target compounds were obtained from the PubChem database (https://pubchem.ncbi.nlm.nih.gov/). Subsequently, molecular docking simulations were conducted using Autodock software to calculate the binding energies between IL-4 and IL-6 with the compounds, considering crucial intermolecular forces such as hydrogen bonds, van der Waals forces, and hydrophobic interactions. Furthermore, Pymol software was employed to analyze hydrogen bonds in the docking results. Based on the absolute values of the molecular docking scores, we evaluated the binding strength between active compounds and targets. A higher binding energy indicates stronger affinity and binding activity between the two entities.

2.3. In vitro and in vivo validation experiments

2.3.1. Experimental cells and animals

The human corneal epithelial cell line HCE-T was obtained from Ubigene (ubigene.com). Cells were cultured in Minimum Essential Medium (MEM, Thermo Fisher, 11095080) supplemented with 10 % fetal bovine serum (FBS, Gibco, 10099141C) and penicillin-streptomycin (Gibco, 15140122). Fifteen female Balb/c mice (5 weeks old, 15–25 g) were purchased from Shanghai Sipubikai Laboratory Animal Co., Ltd. All mice were housed under standard laboratory conditions at a constant temperature (23 ± 1)℃, relative humidity of 40 %–60 %, and a 12 h light/12 h dark cycle. Animal experiments, including euthanasia procedures, were conducted in strict accordance with the guidelines of the Shanghai University of Traditional Chinese Medicine and the Association for Research in Vision and Ophthalmology (ARVO). Ethical approval was obtained from the Animal Ethics Committee of Shanghai University of Traditional Chinese Medicine (Approval No.: PZSHUTCM190222039).

2.3.2. Drug affinity responsive target stability (DARTS)

The DARTS assay was performed as previously described (Qu et al., 2023; Xue et al., 2023). Briefly, cells were collected and lysed using M-PER lysis buffer (Thermo Fisher, 78501) supplemented with a complete protease inhibitor (Roche, 04693124001) and a phosphatase inhibitor (Roche, 04906845001). The lysates were diluted with TNC buffer and aliquoted into 1.5 mL tubes. Samples were incubated with 2 μM luteolin or an equal volume of DMSO at room temperature for 1 h. Following incubation, 1 μg of pronase (MCE, HY-114158A) was added to 300 μg of lysate for digestion over 30 min. The reaction was terminated by adding a protein loading buffer and heating the samples. Western blot analysis was then performed to assess protein stability.

2.3.3. Animal modeling, grouping, and drug administration

The 15 BALB/c mice were randomly divided into the control (Naive) group, recurrent model (Re) group, and YQJD formula group, with 5 mice in each group. According to the method described in the literature, skilled surgeons precisely scraped the corneas of mice in the Re group and YQJD group under a microscope, penetrating moderately into the corneal epithelium or superficial stroma (Morris et al., 2012). The control group received 5 μL of saline treatment in the eye, while the Re and YQJD groups received 5 μL of suspension of HSV-1 (1×10^6 PFU) treatment. After 3 weeks of modeling, the mice in the YQJD group received oral medication (0.2 ml/10 g) twice daily for 5 weeks. The Naive and Re group mice received an equivalent dose of saline orally. After the treatment, mice were anesthetized with 1 % pentobarbital sodium solution, and their eye tissues were collected. Five weeks after the initial infection, the corneas of mice were examined using a slit lamp. Following the spontaneous resolution of HSK, only the right eyes of mice in the recurrent and YQJD groups underwent an optimal duration of exposure to ultraviolet light (UV-B-302 nm) as the treatment for the HSK recurrence model. The control group received no treatment. The eyes of the mice were observed, stained, photographed, and evaluated before and after UV light exposure.

2.3.4. Fluorescein sodium staining

This study employed the Fluorescein sodium staining technique to assess corneal damage and alterations in mice. Specifically, a 0.1 % fluorescein sodium solution was prepared and instilled into the eyes of mice under general anesthesia, allowing the solution to naturally cover the corneal surface. Subsequently, post-staining, the corneal transparency, neovascularization, and any injuries or defects were observed and recorded using a fluorescence microscope with a blue light filter. This method enabled a clear evaluation and comparison of the effects of the Re group and YQJD treatment group in improving corneal lesions.

2.3.5. Hematoxylin and eosin (HE) staining

Eye tissues were fixed in 4 % paraformaldehyde solution, and 8 μm-thick sections were prepared. Dehydration and embedding in paraffin were performed using a specialized dehydrating instrument to ensure tissue structure stability. Following pretreatment, tissue blocks were embedded, sectioned, and baked to remove excess water and wax. Standard deparaffinization and clearing procedures were carried out on the sections. Subsequently, HE staining was conducted using an HE staining kit (Zhuhai Besee Biotechnology Co., Ltd., BA-4226), and the corneal tissue's pathological changes were evaluated under an optical microscope.

2.3.6. RT-PCR

Total RNA was extracted using Trizol reagent, followed by homogenization for 1 min using a tissue disruptor and then left at room temperature for 10 min. Subsequently, 200 μL of chloroform was added, thoroughly mixed, and centrifuged at 15,000 rpm for 5–7 min. The supernatant was transferred to a new tube, mixed with 600 μL of chloroform, and centrifuged again. Afterwards, the supernatant was mixed with 500 μL isopropyl alcohol to precipitate RNA, then centrifuged to remove the supernatant, washed the RNA pellet with 75 % ethanol, and centrifuged again. The RNA pellet was air-dried for 2-3 min and dissolved in RNase-free water. Quantification was performed by measuring the OD260 of 1 μL of total RNA. Primers and sequences were designed based on gene sequences from the GenBank database (Table S3) and optimized using NCBI Primer-BLAST, with the primers synthesized by Suzhou Jinyi Company. Following reverse transcription, polymerase chain reaction (PCR) amplification was carried out, and upon

completion of the reaction, data analysis was conducted to determine the levels of IL-6 mRNA, IL-4 mRNA, PI3K mRNA, and AKT mRNA.

2.3.7. Western blot

Total protein was extracted using a commercial kit, and protein concentration was determined with a BCA assay (Thermo Fisher Scientific). Equal amounts of protein were separated by 10 % SDS-PAGE and transferred onto PVDF membranes. After blocking with 5 % non-fat milk for 1 h at room temperature, membranes were incubated overnight at 4 ℃ with primary antibodies against PI3 Kinase P85, Phospho-PI3 Kinase P85 (Tyr458)/p55 (Tyr199), Akt, Phospho-Akt (Ser473), Phospho-NF-κB p65 (Ser536), NF-κB p65, IL-4, and β-Actin (loading control) (Cell Signaling Technology, USA). Insulin-like Growth Factor-1 (IGF-1, a PI3K agonist; purchased from Sigma Chemical) was used to validate the involvement of the PI3K/Akt signaling pathway in the therapeutic effects of YQJD. The IGF group received combined treatment with IGF-1 and YQJD. After incubation with HRP-conjugated secondary antibodies at room temperature, protein bands were visualized using an enhanced chemiluminescence (ECL) detection reagent and quantified with ImageJ software, with β-actin as the internal reference. The PI3K agonist IGF-1 was purchased from Sigma Chemical (Shang et al., 2023).

2.3.8. Cell modeling and grouping

HSV-1 viral stock was diluted following the method reported previously (Shah et al., 2010) and used to infect Human Corneal Epithelial Cells (HCECs) at a concentration of 1.0 PFU/cell. After 36 h of cultured HCECs at 37 °C, YQJD formula serum, blank serum (Re), and fresh culture medium (Naive) were individually added to the cell cultures, followed by an additional 12 h of incubation. Subsequently, a single wash with 1×PBS was performed to remove the unbound virus. The cells were then treated with varying concentrations of HSV-1 virus (0.01 PFU/cell, 0.001 PFU/cell). Cells and supernatants were collected after incubating the cells at 37 °C for 6 and 18 h. For detailed cell grouping, refer to Table 1.

2.3.9. Cell counting kit-8 (CCK-8) assay

Cell viability was assessed using the CCK-8 assay. HCE-T cells were seeded in 96-well plates at a density of 8000 cells/well and incubated with YQJD-containing serum at different concentrations (2.5 %, 5 %, 10 %, and 20 %) for 24 h, while the control group received serum-free medium. CCK-8 solution (10 μL/well) (Beyotime, Shanghai, China) was added, and plates were incubated at 37 °C for 4 h. Absorbance was measured at 450 nm. All experiments were performed in triplicate, and data were summarized for graphical representation (Zhang et al., 2022).

2.3.10. ELISA

In this study, the expression levels of IL-4 in the supernatant of HCECs were quantitatively detected using the ELISA kit (Boster Bio, EK0404). This procedure strictly adhered to the standardized protocol provided by the manufacturer, ensuring the reliability and accuracy of the experimental data.

Table 1
Cell culture grouping (6 h and 18h).

Group	Number of Wells
0.01PFU/cell Drug Serum 6 h	3
0.001 PFU/cell Drug Serum 6 h	3
0.01 PFU/cell Blank Serum 6 h	3
0.001 PFU/cell Blank Serum 6 h	3
0.01 PFU/cell No Serum 6 h	3
0.001 PFU/cell No Serum 6 h	3
0.001 PFU/cell Drug Serum 18 h	3
0.001 PFU/cell Blank Serum 18 h	3
0.001 PFU/cell No Serum 18 h	3

2.3.11. Immunofluorescence

Approximately 1-2×10^4 HCE-T cells were seeded onto coverslips and pre-incubated for 5 h to allow adhesion. Subsequently, 1 mL of culture medium was gently added, and cells were incubated overnight at 37 °C. The following day, cells were fixed with 4 % paraformaldehyde, blocked with bovine serum albumin (BSA) for 30 min, and incubated overnight at 4°C with an IL-4 antibody (Ruibo Biology, R0005, 1:400). After washing, a secondary antibody (1:500) was applied and incubated at 37 °C in the dark for 2 h. Cell nuclei were stained with DAPI, and after PBS washes, slides were mounted with an anti-fade mounting medium and imaged using a fluorescence microscope.

2.4. Statistical analysis

Data analysis was performed using SPSS 26 software, and GraphPad Prism 8.0 was used for graphical representation. For continuous variables, if data in each group followed a normal distribution (confirmed by the Shapiro-Wilk test), a one-way analysis of variance (ANOVA) was used to compare multiple groups. Post-hoc comparisons were conducted using the LSD test for homoscedasticity and the Games-Howell test for heteroscedasticity. In cases where the data did not adhere to a normal distribution, non-parametric tests were applied. The results were presented as mean ± standard deviation, with a p-value < 0.05 indicating statistical significance.

3. Results

3.1. Analysis of YQJD formula by UPLC-Q-Orbitrap HRMS

Utilizing the UPLC-Q-Orbitrap HRMS technology in this study, 34 main compounds were identified in the YQJD formula. Detailed mass spectra depicting the chromatographic distribution and characteristic ion peaks of the compounds are shown in Fig. 1A and B. The chromatogram in Fig. 1A illustrates compounds such as gluconic acid and quinic acid with early elution peaks, while Fig. 1B depicts complex components identified in later analysis, such as saikosaponin D. By matching the accurate masses and fragment ion spectra of chromatographic peaks, multiple compounds including citric acid, caffeic acid, uridine, chlorogenic acid, and their isomers were successfully identified. After screening for oral bioavailability (OB) ≥30 % and drug-likeness (DL) ≥ 0.18, two compounds (Isovitexin, Formononetin) met the criteria.

3.2. Pharmacological network analysis results

3.2.1. Active ingredients and targets of YQJD formula

The herbal composition of YQJD includes Huang Qi, Bai Zhu, Fang Feng, Jin Yin Hua, Pu Gong Ying, Da Qing Ye, Zi Cao, Chan Tui, Fu Ling, Sheng Di Huang, and Chai Hu. By systematically querying the TCMSP and BATMAN-TCM databases, the active ingredients (Fig. 2A) and target proteins (Fig. 2B) of the YQJD formula were identified. Notably, the 96 active ingredients mainly consist of Mairin, Jaranol, 3,9-Di-O-methylnissolin, Formononetin, and Isoflavanone, as detailed in Table 2.

3.2.2. Key targets for treating HSK with YQJD

Considering the potential recurrence of immune and inflammatory responses leading to corneal damage, which serves as a pivotal target for HSK treatment, this study focused on four key terms: "Herpes Simplex Keratitis," "corneal opacity," "corneal scarring," and "corneal injury (inflammatory)" for in-depth analysis. The HSK targets were retrieved from the OMIM and GeneCards databases (Fig. 2C). The intersection targets between YQJD and HSK comprised 97 elements (Fig. 2D).

3.2.3. GO and KEGG analysis

A GO and KEGG analysis was conducted on the 97 key targets. In the BP category, the analysis primarily involved positive regulation of gene

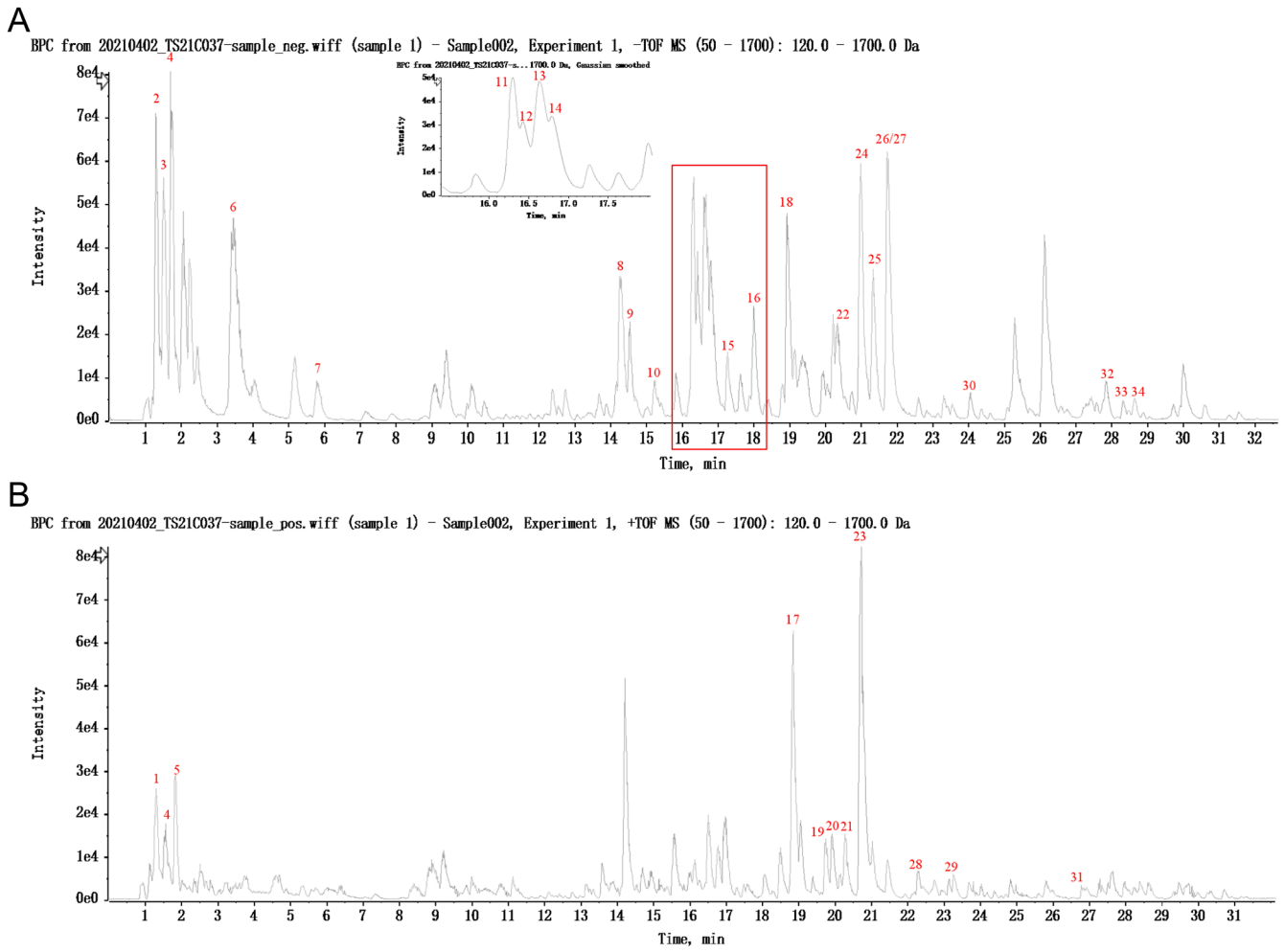

Fig. 1. UPLC-Q-Orbitrap HRMS analysis of the YQJD formula.
Note: (A) Base peak chromatogram (BPC) of the sample in negative ion mode using UHPLC-HRMS. (B) The BPC of the sample is in positive ion mode using UHPLC-HRMS.

expression, negative regulation of apoptotic processes, and positive regulation of transcription from RNA polymerase II promoter. In the MF category, the findings focused on protein binding, identical protein binding, and enzyme binding. The CC category mainly included the extracellular region, cytoplasm, and plasma membrane (Fig. 2E and G).

The KEGG pathway analysis unveiled diverse biological signaling pathways, with the PI3K/Akt signaling pathway being one of the most significant routes. Additionally, pathways such as Pathways in Cancer, Human Cytomegalovirus Infection, Lipid and Atherosclerosis, Proteoglycans in Cancer, and the MAPK signaling pathway were also identified (Fig. 2F).

3.2.4. YQJD anti-HSK active formulas and targets based on multidimensional network

Using Cytoscape software, this study successfully constructed and visually depicted a multidimensional "Formula-Compound-Target-Disease (F-C-T-D)" integrated network (Fig. 3). The aim was to screen potential active components and target proteins of the YQJD formula for improving corneal inflammation. Through this network analysis, we identified several active compounds including 3-Methyl-2-(2-penten-1-yl)-2-cyclopenten-1-one, 6-(3-hydroxyindol-2-ylmethyl)indolo[2,1-b] quinoxaline-12-one, and dimethyl caffeate, along with targets such as IL-4, IL-6, brain-derived neurotrophic factor (BDNF), and vascular endothelial growth factor A (VEGFA).

3.2.5. Molecular docking

The STRING database was used to construct a PPI network, identifying key genes downstream of the PI3K/Akt signaling pathway to establish a theoretical basis for molecular docking analyses. In this network, darker node colors indicate stronger associations with other genes. Among the identified targets, NF-κB1, IL-4, IL-6, FGFR2, TP53, and BCL2 emerged as the most central. The literature review confirmed IL-4 and IL-6 as pivotal genes for molecular docking analysis (Fig. 4).

Molecular docking analysis was performed to predict the binding mechanisms and affinities between active compounds and target proteins. Binding activity was classified based on docking scores: values below −4.25 kJ/mol suggest potential binding, below −5.0 kJ/mol indicate strong binding, and below −7.0 kJ/mol represent high-affinity interactions (Hsin et al., 2013). The results showed that IL-4 and IL-6 exhibited strong binding affinities with luteolin, hydrangeic acid, and thymol. Table 3 presents the binding energies of IL-4 and IL-6 with various compounds, highlighting interaction types such as hydrogen bonding, van der Waals forces, and hydrophobic interactions.

PyMOL software was used to analyze hydrogen bond interactions between IL-4, IL-6, and active compounds (Fig. 5A, D), with hydrogen bonds considered a key indicator of binding affinity. DARTS was employed to further validate the molecular docking results, a technique that confirms ligand-target interactions by assessing the reduced proteolytic sensitivity of the target protein upon ligand binding (Lomenick et al., 2009). The results demonstrated that luteolin enhanced the

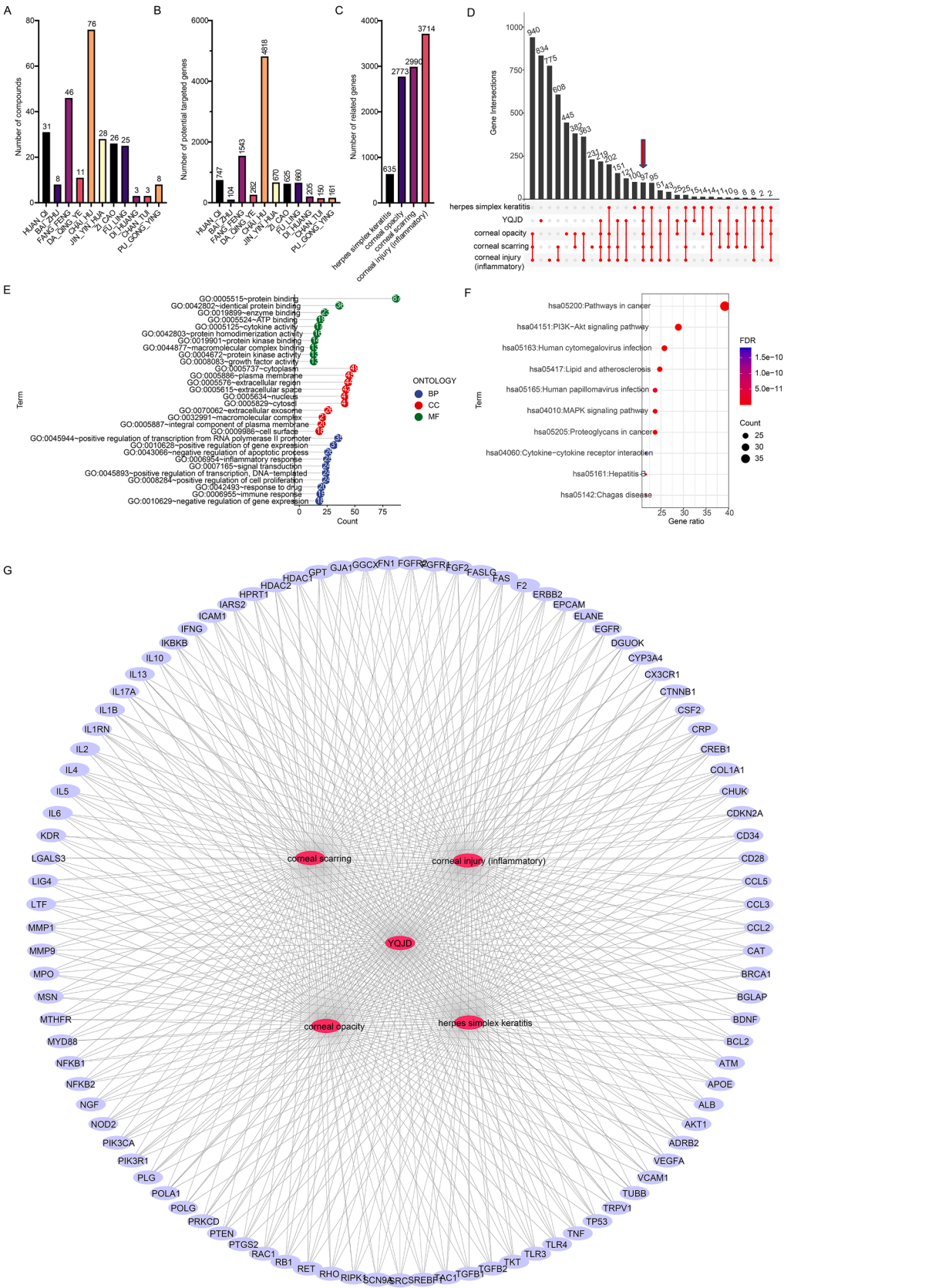

Fig. 2. Key targets and related functional and pathway analyses in treating HSK with YQJD formula.
Note: (A) Number of active components in the YQJD formula. (B) Number of targets of the YQJD formula. (C) Several HSK targets. (D) The upset plot shows the intersection of genes between YQJD and HSK. (E) Functional analysis of 97 intersection genes. (F) Enrichment analysis of KEGG pathways. (G) PPI network of 97 intersecting genes.

Table 2
YQJD formula components.

Mol ID	Molecule Name	OB (%)	DL
MOL000211	Mairin	55.38	0.78
MOL000239	Jaranol	50.83	0.29
MOL000371	3,9-di-O-methylnissolin	53.74	0.48
MOL000374	5′-hydroxyiso-muronulatol-2′,5′-di-O-glucoside	41.72	0.69
MOL000378	7-O-methylisomucronulatol	74.69	0.3
MOL000379	9,10-dimethoxypterocarpan-3-O-β-D-glucoside	36.74	0.92
MOL000380	(6aR,11aR)-9,10-dimethoxy-6a,11a-dihydro-6H-benzofurano[3,2-c]chromen-3-ol	64.26	0.42
MOL000387	Bifendate	31.1	0.67
MOL000392	formononetin	69.67	0.21
MOL000398	isoflavanone	109.99	0.3
MOL000417	Calycosin	47.75	0.24
MOL000020	12-senecioyl-2E,8E,10E-atractylentriol	62.4	0.22
MOL000021	14-acetyl-12-senecioyl-2E,8E,10E-atractylentriol	60.31	0.31
MOL000022	14-acetyl-12-senecioyl-2E,8Z,10E-atractylentriol	63.37	0.3
MOL000028	α-Amyrin	39.51	0.76
MOL000049	3β-acetoxyatractylone	54.07	0.22
MOL000072	8β-ethoxy atractylenolide III	35.95	0.21
MOL000011	(2R,3R)-3-(4-hydroxy-3-methoxy-phenyl)-5-methoxy-2-methylol-2,3-dihydropyrano[5,6-h][1,4]benzodioxin-9-one	68.83	0.66
MOL011730	11-hydroxy-sec-o-beta-d-glucosylhamaudol_qt	50.24	0.27
MOL011732	anomalin	59.65	0.66
MOL011737	divaricatacid	87	0.32
MOL011740	divaricatol	31.65	0.38
MOL001941	Ammidin	34.55	0.22
MOL011747	ledebouriellol	32.05	0.51
MOL011749	phelloptorin	43.39	0.28
MOL011753	5-O-Methylvisamminol	37.99	0.25
MOL002644	Phellopterin	40.19	0.28
MOL000173	wogonin	30.68	0.23
MOL001942	isoimperatorin	45.46	0.23
MOL003588	Prangenidin	36.31	0.22
MOL007514	methyl icosa-11,14-dienoate	39.67	0.23
MOL013077	Decursin	39.27	0.38
MOL001495	Ethyl linolenate	46.1	0.2
MOL002707	phytofluene	43.18	0.5
MOL002914	Eriodyctiol (flavanone)	41.35	0.24
MOL003006	(-)-(3R,8S,9R,9aS,10aS)-9-ethenyl-8-(beta-D-glucopyranosyloxy)-2,3,9,9a,10,10a-hexahydro-5-oxo-5H,8H-pyrano[4,3-d]oxazolo[3,2-a]pyridine-3-carboxylic acid_qt	87.47	0.23
MOL003014	secologanic dibutylacetal_qt	53.65	0.29
MOL002773	beta-carotene	37.18	0.58
MOL003036	ZINC03978781	43.83	0.76
MOL003044	Chryseriol	35.85	0.27
MOL003059	kryptoxanthin	47.25	0.57
MOL003062	4,5′-Retro-.beta.,.beta.-Carotene-3,3′-dione, 4′,5′-didehydro-	31.22	0.55
MOL003095	5-hydroxy-7-methoxy-2-(3,4,5-trimethoxyphenyl)chromone	51.96	0.41
MOL003101	7-epi-Vogeloside	46.13	0.58
MOL003108	Caeruloside C	55.64	0.73
MOL003111	Centauroside_qt	55.79	0.5
MOL003117	Ioniceracetalides B_qt	61.19	0.19
MOL003124	XYLOSTOSIDINE	43.17	0.64
MOL003128	dinethylsecologanoside	48.46	0.48
MOL000006	luteolin	36.16	0.25
MOL001771	poriferast-5-en-3beta-ol	36.91	0.75
MOL001781	Indigo	38.2	0.26
MOL001810	6-(3-oxoindolin-2-ylidene)indolo[2,1-b]quinazolin-12-one	45.28	0.89
MOL002308	Indicaxanthin	31.79	0.22
MOL002309	indirubin	48.59	0.26
MOL002311	Glycyrol	90.78	0.67
MOL002318	C05837	66.02	0.48
MOL002320	γ-sitosterol	36.91	0.75
MOL002322	isovitexin	31.29	0.72
MOL002372	(6Z,10E,14E,18E)-2,6,10,15,19,23-hexamethyltetracosa-2,6,10,14,18,22-hexaene	33.55	0.42
MOL002883	Ethyl oleate (NF)	32.4	0.19
MOL007714	1-methoxyacetylshikonin	73.09	0.29
MOL007715	[(1R)-1-(5,8-dihydroxy-1,4-dioxo-2-naphthyl)-4-methyl-pent-3-enyl] propanoate	54.64	0.29
MOL007716	acetylshikonin	62.39	0.27
MOL007722	Isoarnebin 4	64.79	0.2
MOL007728	lithospermidin A	75.08	0.38
MOL007734	5-[(E)-5-(3-furyl)-2-methyl-pent-2-enyl]-2,3-dimethoxy-p-benzoquinone	61.8	0.24
MOL007735	Des-O-methyllasiodiplodin	30.12	0.2
MOL007736	Lithospermidin B	60.48	0.39
MOL000273	(2R)-2-[(3S,5R,10S,13R,14R,16R,17R)-3,16-dihydroxy-4,4,10,13,14-pentamethyl-2,3,5,6,12,15,16,17-octahydro-1H-cyclopenta[a]phenanthren-17-yl]-6-methylhept-5-enoic acid	30.93	0.81
MOL000275	trametenolic acid	38.71	0.8
MOL000276	7,9(11)-dehydropachymic acid	35.11	0.81
MOL000279	Cerevisterol	37.96	0.77
MOL000280	(2R)-2-[(3S,5R,10S,13R,14R,16R,17R)-3,16-dihydroxy-4,4,10,13,14-pentamethyl-2,3,5,6,12,15,16,17-octahydro-1H-cyclopenta[a]phenanthren-17-yl]-5-isopropyl-hex-5-enoic acid	31.07	0.82
MOL000282	ergosta-7,22E-dien-3beta-ol	43.51	0.72
MOL000283	Ergosterol peroxide	40.36	0.81
MOL000285	(2R)-2-[(5R,10S,13R,14R,16R,17R)-16-hydroxy-3-keto-4,4,10,13,14-pentamethyl-1,2,5,6,12,15,16,17-octahydrocyclopenta[a]phenanthren-17-yl]-5-isopropyl-hex-5-enoic acid	38.26	0.82
MOL000287	3beta-Hydroxy-24-methylene-8-lanostene-21-oic acid	38.7	0.81
MOL000289	pachymic acid	33.63	0.81
MOL000290	Poricoic acid A	30.61	0.76
MOL000291	Poricoic acid B	30.52	0.75
MOL000292	poricoic acid C	38.15	0.75
MOL000300	dehydroeburicoic acid	44.17	0.83
MOL001645	Linoleyl acetate	42.1	0.2
MOL002776	Baicalin	40.12	0.75
MOL004598	3,5,6,7-tetramethoxy-2-(3,4,5-trimethoxyphenyl)chromone	31.97	0.59
MOL004609	Areapillin	48.96	0.41
MOL013187	Cubebin	57.13	0.64
MOL004624	Longikaurin A	47.72	0.53
MOL004628	Octalupine	47.82	0.28
MOL004644	Sainfuran	79.91	0.23
MOL004648	Troxerutin	31.6	0.28
MOL004653	(+)-Anomalin	46.06	0.66
MOL004702	saikosaponin c_qt	30.5	0.63
MOL004718	α-spinasterol	42.98	0.76
MOL000490	petunidin	30.05	0.31

protease resistance of IL-4, providing strong evidence for a direct interaction with IL-4 (Fig. 5B, C).

3.3. Fluorescein sodium and HE staining for the assessment of corneal lesions in mice and the therapeutic effect of YQJD

Fluorescein sodium staining revealed that the control group mice exhibited normal corneal transparency with no significant staining or neovascularization on the ocular surface. In contrast, mice in the Re group demonstrated a significant decrease in corneal transparency, presenting as punctate and patchy corneal opacities with noticeable neovascularization. The corneal transparency in the YQJD group mice was significantly better than in the Re group, showing reduced neovascularization and no obvious damage on the corneal surface (Fig. 6A).

HE staining of corneal tissues in mice showed that the corneal epithelium in the control group mice remained intact, without inflammatory cell infiltration, with even corneal thickness, indicating no significant pathological changes. In contrast, mice in the Re group exhibited epithelial cell degeneration, necrosis, shedding, congestion and edema in the cornea, and significant inflammatory cell infiltration

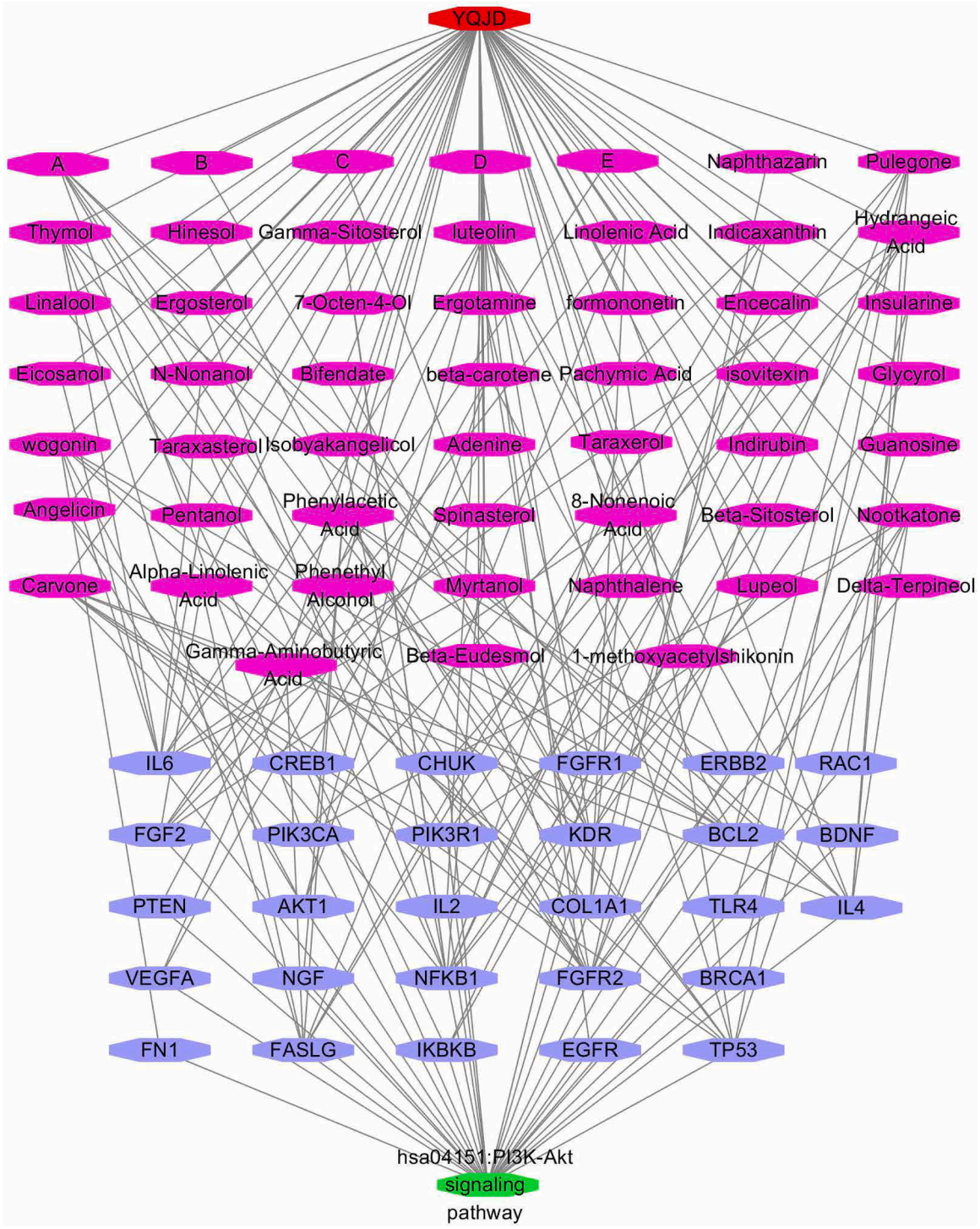

Fig. 3. Integrated "formula-compound-target-disease" network for YQJD treatment of HSK.
Note: This figure depicts the integration network of YQJD formula in treating Herpes Simplex Keratitis (HSK). Red nodes represent the YQJD formula, pink nodes denote the active compounds within the formula, blue nodes indicate the target proteins of these compounds, and green nodes represent crucial signaling pathways (such as the PI3K-Akt pathway).

(+++). On the other hand, although local thickening of the corneal epithelium was observed in the YQJD group mice (+), no epithelial cell necrosis or significant inflammatory cell infiltration was evident (Fig. 6B).

3.4. Effects of YQJD on Corneal inflammatory factors and signaling pathways in Re group mice

This study investigated the effects of YQJD on corneal inflammatory factors IL-4, IL-6, and signaling molecules AKT and PI3K in Re group mice. RT-PCR analysis showed that compared to the control group, IL-4 mRNA expression was significantly reduced in the Re group, whereas YQJD treatment markedly increased its expression ($P < 0.05$) (Fig. 7A).

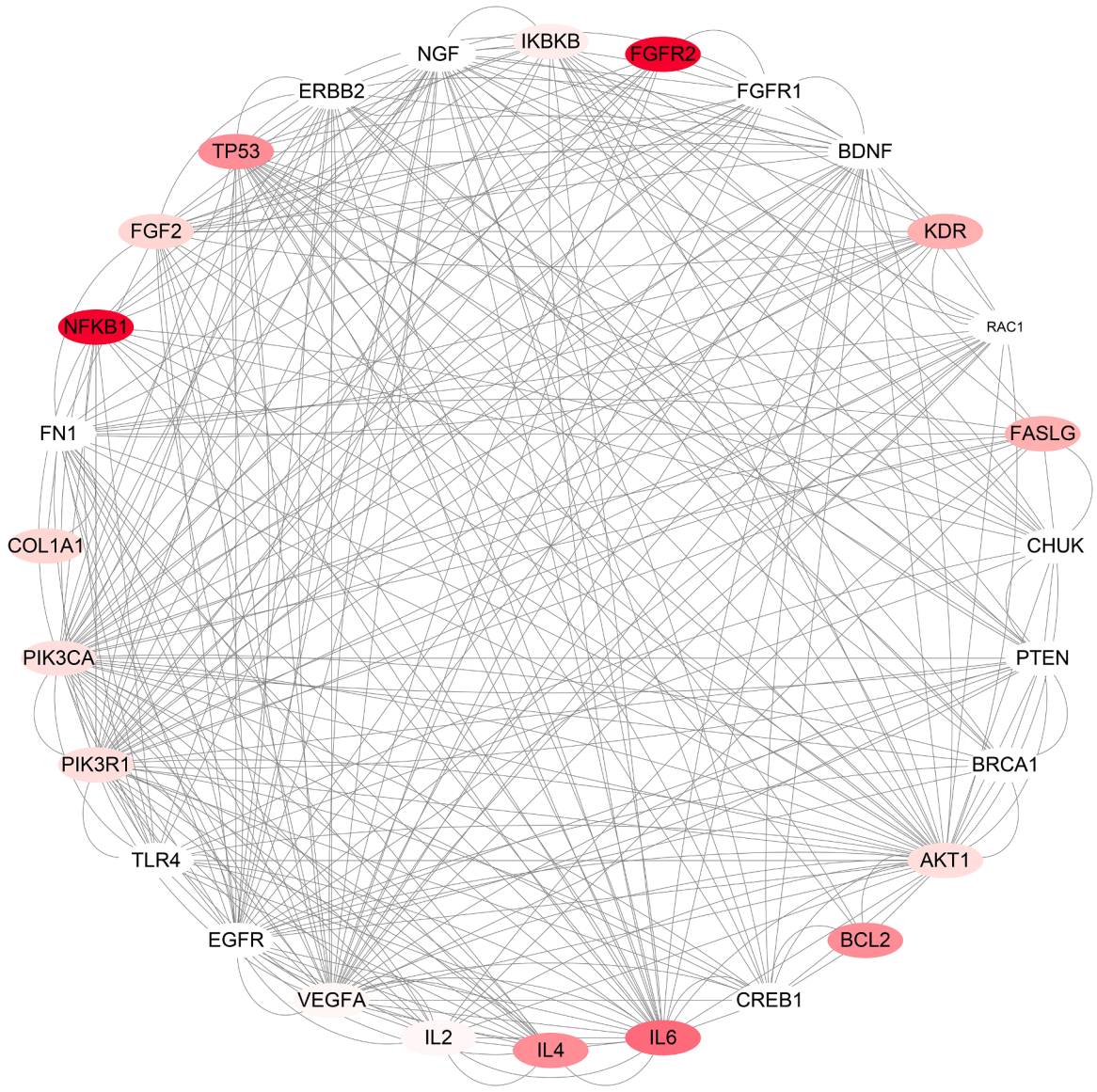

Fig. 4. PPI network of key genes downstream of the PI3K/Akt signaling pathway.

Table 3
Binding of IL4 and IL6 to the compounds.

Compound	Genes	Affinity (kcal/mol)
luteolin	IL4	-7.0
formononetin	IL4	-6.6
Hydrangeic Acid	IL4	-6.5
Nootkatone	IL4	-6.2
Carvone	IL4	-5.2
Thymol	IL4	-4.9
Pulegone	IL4	-4.9
3-Methyl-2-(2-Pentenyl)-2-Cyclopenten-1-One	IL4	-4.8
luteolin	IL6	-6.8
Hydrangeic Acid	IL6	-6.1
wogonin	IL6	-5.9
Thymol	IL6	-4.5
Phenylacetic Acid	IL6	-4.5
Myrtanol	IL6	-4.5
N-Nonanol	IL6	-3.4
Pentanol	IL6	-3.3
Eicosanol	IL6	-3.0

Conversely, IL-6 mRNA and AKT mRNA levels were significantly elevated in the Re group but were significantly reduced after YQJD treatment ($P < 0.01$) (Fig. 7B, D). No significant differences were observed in PI3K mRNA expression among groups (Fig. 7C).

Western blot analysis was conducted to evaluate the activation status of the PI3K/AKT signaling pathway. Following viral infection, p-PI3K, AKT, and p-AKT expression levels were significantly increased, whereas YQJD treatment effectively suppressed their expression (Fig. 7E–I). The inhibitory effect of YQJD on this pathway was reversed upon PI3K agonist administration, but PI3K total protein expression remained unchanged, consistent with the RT-PCR findings.

Given that the PI3K/AKT pathway plays a crucial role in inflammatory responses and is closely linked to NF-κB signaling, the expression levels of p-NF-κB and NF-κB were further examined. The results demonstrated that YQJD also inhibited NF-κB phosphorylation (Fig. 7J), suggesting that its anti-inflammatory effects may be mediated via suppression of the PI3K/AKT/NF-κB axis.

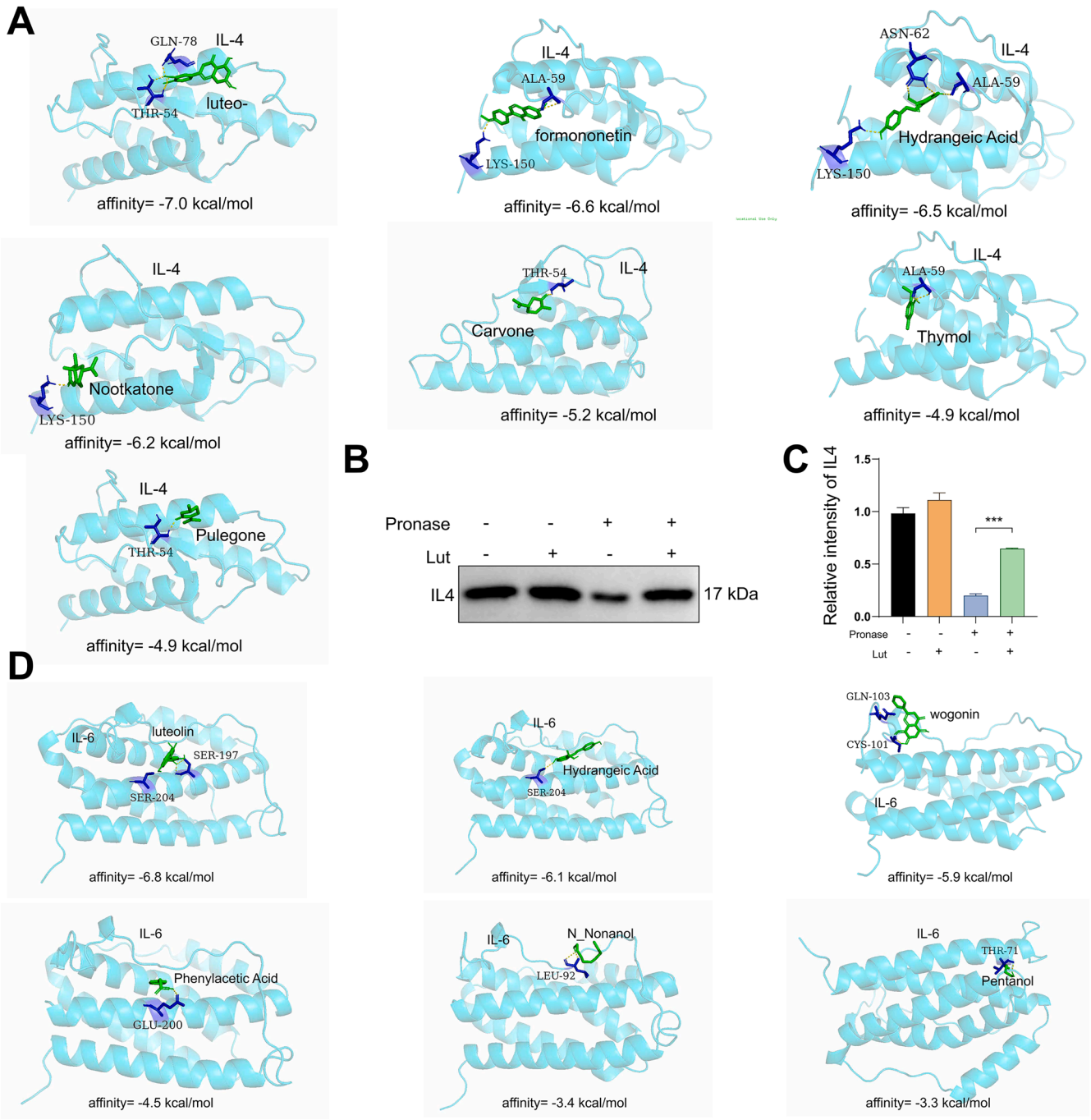

Fig. 5. Affinity and binding site analysis of IL-4 and IL-6 with various active components.
Note: (A) Binding analysis of IL-4 with active components: Luteolin: Affinity -7.0 kcal/mol; Formononetin: Affinity -6.6 kcal/mol; Hydrangeic Acid: Affinity -6.5 kcal/mol; Nootkatone: Affinity -6.2 kcal/mol; Carvone: Affinity -5.2 kcal/mol; Thymol: Affinity -4.9 kcal/mol; Pulegone: Affinity -4.9 kcal/mol. (B) DARTS assay evaluating the effect of luteolin on IL-4 proteolytic sensitivity. (C) IL-4 protein band density analysis. (D) Binding analysis of IL-6 with active components: Luteolin: Affinity -6.8 kcal/mol; Hydrangeic Acid: Affinity -6.1 kcal/mol; Wogonin: Affinity -5.9 kcal/mol; Phenylacetic Acid: Affinity -4.5 kcal/mol; N-Nonanol: Affinity -3.4 kcal/mol; Pentanol: Affinity -3.3 kcal/mol.

3.5. Impact of drug-containing serum on IL-4 expression in HCECs infected with HSV-1

IL-4 is a key target of YQJD in HSK treatment (Fig. 4). This study further investigated the effect of YQJD-containing serum on IL-4 expression in HSV-1-infected HCECs. CCK-8 assay results showed that at 24 h, cell viability significantly decreased in the 10 % YQJD and 20 % YQJD groups ($P < 0.05$, $P < 0.01$) (Fig. 8A). At 48 h, cell viability was significantly reduced in the 5 %, 10 %, and 20 % YQJD groups ($P < 0.05$, $P < 0.01$, $P < 0.01$) (Fig. 8B). No significant differences were observed in the 2.5 % YQJD group compared to the control, and thus 2.5 % YQJD was selected for subsequent experiments. After 0.01 PFU/cell HSV-1 infection of HCECs for 6 h, IL-4 expression in the supernatant was significantly lower in the blank serum (Re) group than in the serum-free (Naive) group, whereas YQJD treatment significantly increased IL-4 expression ($P < 0.01$). At 18 h, IL-4 expression in the Re group was higher than in the Naive group ($P < 0.05$), but no significant differences were observed in the YQJD-treated group. After 0.001 PFU/cell HSV-1

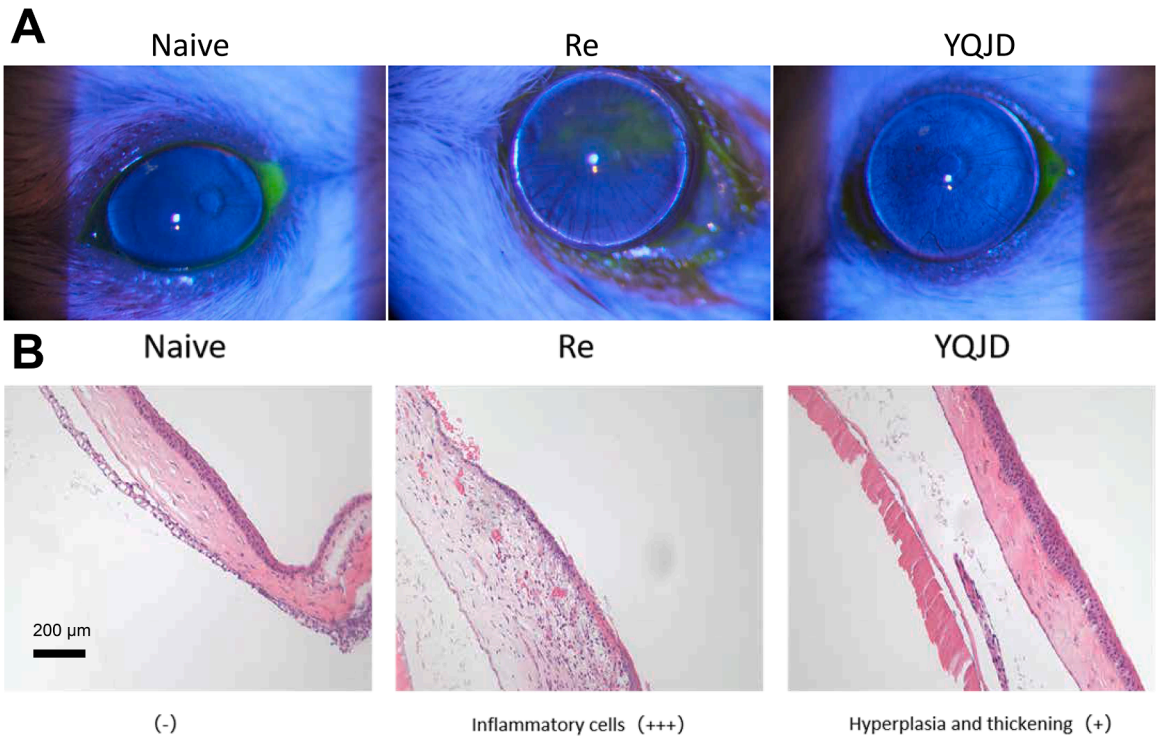

Fig. 6. Observations of mouse corneal staining.
Note: (A) Fluorescein sodium staining of mouse corneas in different groups. (B) HE staining of mouse corneas in different groups (200x magnification).

infection for 6 h or 18 h, IL-4 expression was reduced in the Re group compared to the Naive group, while YQJD treatment significantly increased IL-4 expression ($P < 0.01$) (Fig. 8C). At 0.01 PFU/cell HSV-1 infection, regardless of 6 h or 18 h treatment, IL-4 immunofluorescence intensity in HCECs was significantly higher in the YQJD group than in the Re and Naive groups (Fig. 8D, E).

4. Discussion

The PI3K/Akt signaling pathway is a critical pathway involved in the regulation of cell survival, proliferation, and apoptosis, playing a crucial role in the occurrence and progression of various diseases (Zhang et al., 2022; Sun et al., 2021; Long et al., 2021). Activation of this pathway during HSV-1 infection has dual effects on host cell survival and virus replication. This study demonstrates that the YQJD formula exhibits significant anti-HSV-1 activity by modulating this pathway, similar to drug intervention strategies targeted at this pathway in previous studies (Zhu et al., 2022; Huang et al., 2023). However, unlike single-target drugs, the multi-component and multi-target nature of the YQJD formula as a TCM formulation may lead to broader regulatory effects, a characteristic less commonly reported in existing literature.

IL-4 and IL-6 are pivotal cytokines playing core roles in immune regulation and inflammatory responses (Zhao et al., 2021; Wei et al., 2022; Kuzumi et al., 2021). They play particularly crucial roles in corneal inflammation induced by HSV-1, as their expression levels significantly influence the severity of inflammation and disease progression (Jaggi et al., 2022; Möckel et al., 2022). IL-4 is commonly associated with anti-inflammatory responses, aiding in immune response regulation, while IL-6 is linked to pro-inflammatory processes, with elevated levels commonly observed in various inflammatory and autoimmune diseases. In this study, the application of the YQJD formula markedly upregulated IL-4 expression levels, suggesting its potential to alleviate inflammation by enhancing the activity of anti-inflammatory cytokines (Bryant and Stevens, 2022; Luan et al., 2022; Romo et al., 2023). Meanwhile, the formula reduced IL-6 expression, which helps alleviate inflammation and tissue damage without compromising viral clearance. The ability to simultaneously regulate these two cytokines demonstrates the compound's complex role in modulating immune responses, highlighting significant differences from studies that typically focus on single-drug effects on a single target, revealing the unique advantage of TCM formulations in regulating overall human immune status.

Using UPLC-HRMS, this study identified key YQJD compounds, including citric acid, caffeic acid, and uridine. Based on oral bioavailability (OB ≥30 %) and drug-likeness (DL ≥0.18), Isovitexin and Formononetin were selected for further analysis. Isovitexin exhibits antioxidant, anti-inflammatory, and antimicrobial properties, reducing oxidative stress and inflammatory responses (Naudhani et al., 2021; Teede et al., 2003; Masuda et al., 2021). It also offers cardiovascular protection by mitigating vascular inflammation. Formononetin modulates gut microbiota, improves insulin sensitivity, and reduces arterial stiffness, benefiting metabolic and cardiovascular health (Naudhani et al., 2021; Teede et al., 2003; Masuda et al., 2021). These pharmacological effects may synergistically enhance YQJD's efficacy in HSK by regulating the PI3K/Akt pathway and modulating IL-4 and IL-6 expression. This study not only reinforces existing evidence on the anti-inflammatory and antioxidant mechanisms of these compounds but also highlights their role in cell signaling under HSV-1 pathology. These findings provide a scientific basis for developing natural compound-based antiviral therapies, particularly for viral keratitis and related diseases.

The utilization of network pharmacology methods is progressively demonstrating its unique advantages in modern drug research, particularly in the analysis and interpretation of the multi-component, multi-target action mechanisms of TCM formulations (Zhao et al., 2023; Zheng et al., 2022; Tang et al., 2022). By constructing interaction networks between drug components and disease targets, this approach reveals potential therapeutic mechanisms and identifies new treatment targets (Chen et al., 2019). In this study, network pharmacology was successfully utilized to screen and confirm the active components of the YQJD formula relevant to the treatment of HSK and their target interactions. By analyzing the association between these targets and known

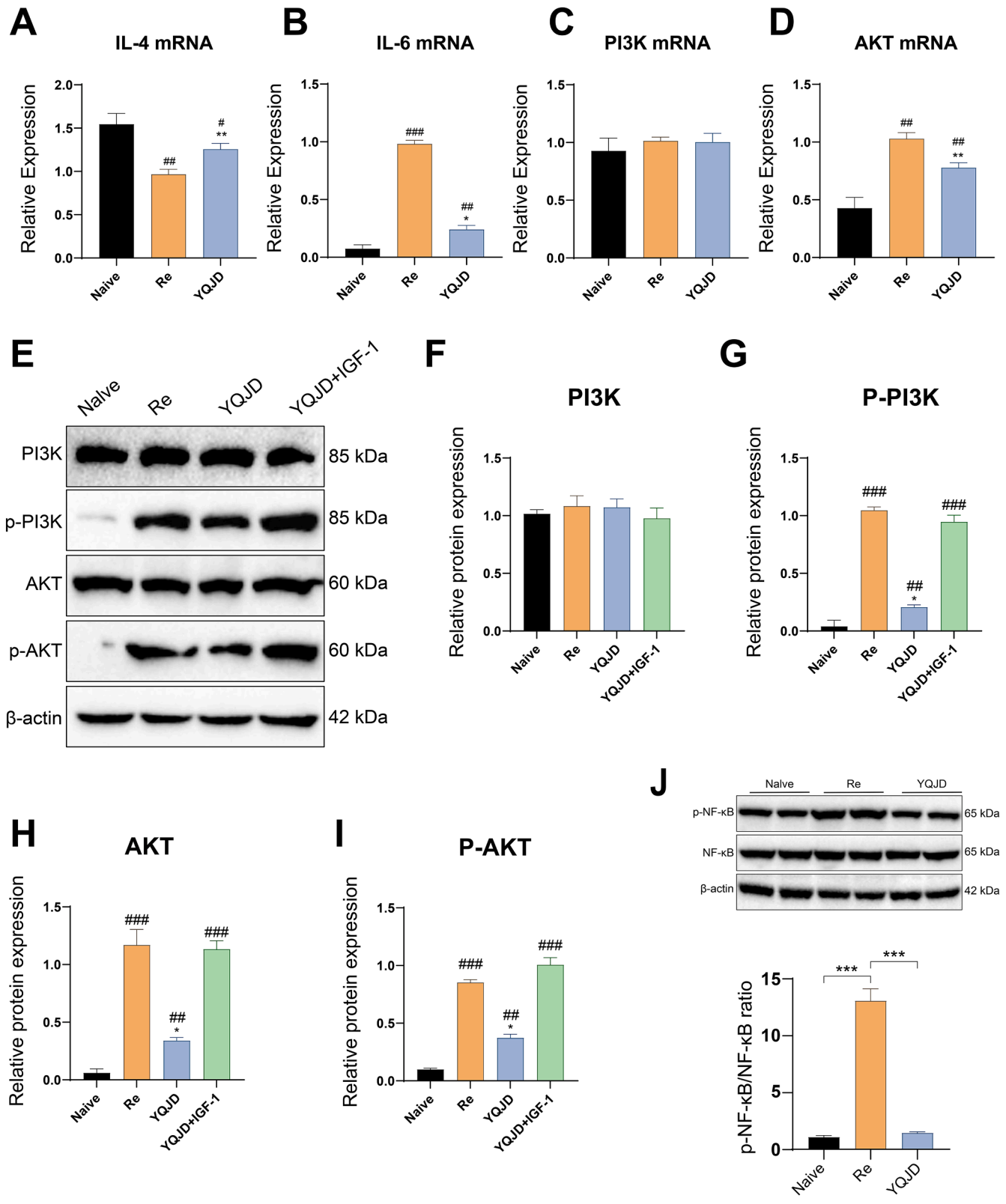

Fig. 7. Expression of PI3K/AKT pathway and inflammatory factors in mouse corneas
Note: (A) IL-4 mRNA expression levels. (B) IL-6 mRNA expression levels. (C) PI3K mRNA expression levels. (D) AKT mRNA expression levels. (E) Expression of PI3K/AKT/NF-κB pathway-related proteins. (F-I) Quantitative analysis of the relative expression levels of PI3K/AKT pathway-related proteins. (J) Expression levels of NF-κB and p-NF-κB in different groups with statistical analysis. # $P < 0.05$, ## $P < 0.01$, ### $P < 0.001$ vs. Naive group; * $P < 0.05$, ** $P < 0.01$ vs. Re group.

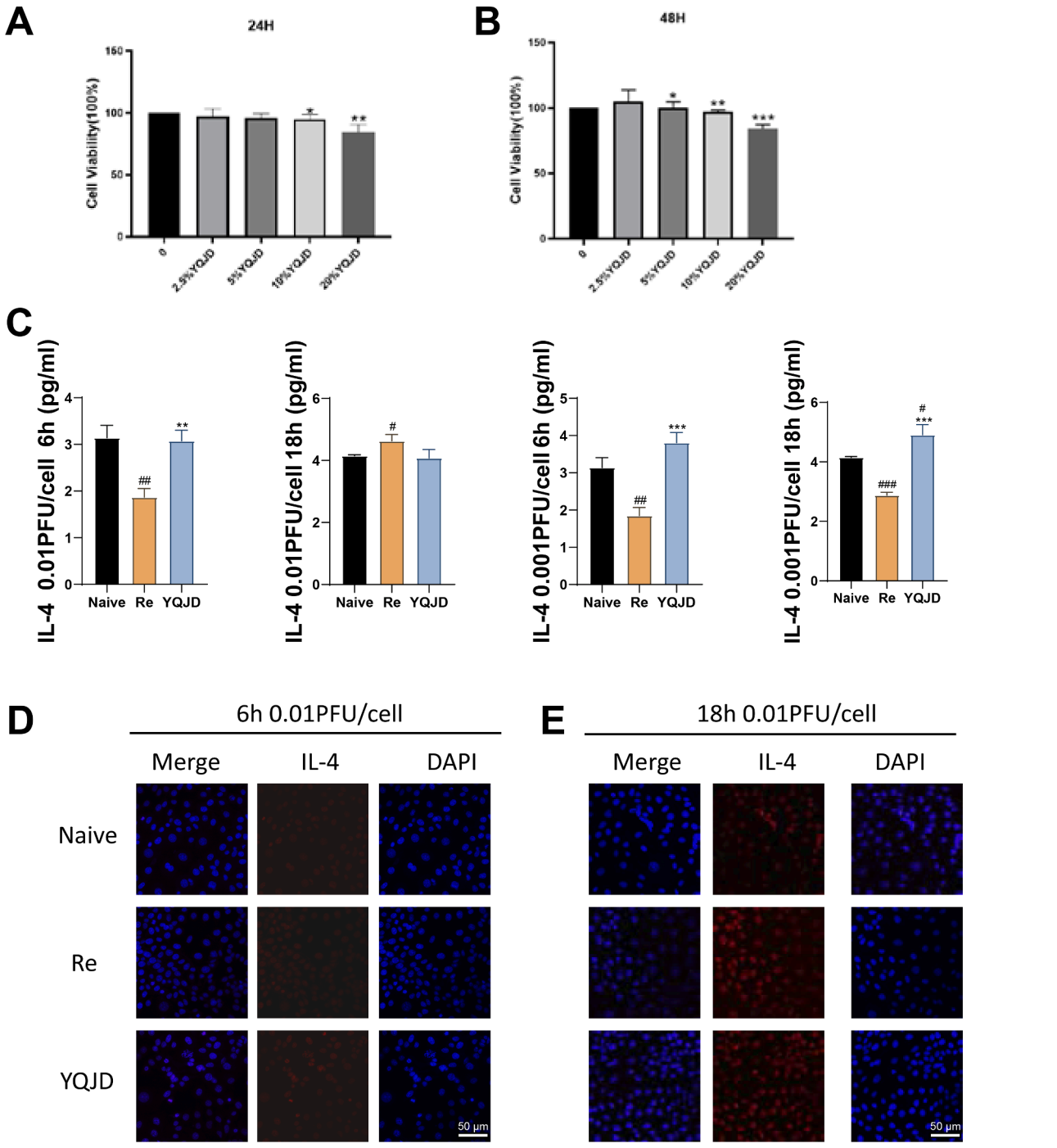

Fig. 8. IL-4 expression levels in HCECs following HSV-1 infection at various concentrations for 6 h and 18 h were detected by ELISA and immunofluorescence. Note: (A) Cell viability of HCECs after 24 h treatment with different concentrations of YQJD (* $P < 0.05$, ** $P < 0.01$, *** $P < 0.001$ vs. untreated group). (B) Cell viability of HCECs after 48 h treatment with different concentrations of YQJD (* $P < 0.05$, ** $P < 0.01$, *** $P < 0.001$ vs. untreated group). (C) IL-4 expression levels in the HCECs supernatant. (D) IL-4 fluorescence expression in HCECs after 6 h of HSV-1 infection. (E) IL-4 fluorescence expression in HCECs after 18 h of HSV-1 infection. # $P < 0.05$, ## $P < 0.01$, ### $P < 0.001$ vs. Naive group; * $P < 0.05$, ** $P < 0.01$, *** $P < 0.001$ vs. Re group.

pathological mechanisms, this study deepens the understanding of the role of the YQJD formula in HSV-1 infection and anti-inflammatory mechanisms. The application of network pharmacology not only enhances research efficiency but also provides a new perspective on understanding drug actions from the molecular to the systemic level, being more comprehensive and systematic compared to traditional efficacy research methods (Li et al., 2022; Scallan and Jannaway, 2022; Parvez et al., 2021).

In traditional and modern medicine, HSV-1 infection and the resulting HSK are typically treated with antiviral drugs and immunomodulators; however, these methods are sometimes limited by drug side effects or limited efficacy (Wang et al., 2023; Jiang et al., 2022; Rousseau et al., 2022). Compared to these therapies, YQJD offers distinct advantages. As a multi-component herbal formula, it exerts multi-target effects, simultaneously suppressing viral replication and alleviating inflammation. Its natural composition may also reduce side effects and improve patient acceptance of synthetic drugs. Furthermore, the synergistic interactions among its compounds may enhance antiviral and

anti-inflammatory activity through mechanisms yet to be fully elucidated. These properties underscore the potential of YQJD as an alternative or adjunct therapy and provide new directions for anti-HSV-1 drug development.

Given the potent antiviral and anti-inflammatory effects demonstrated by the YQJD formula in this study, there is great interest in its clinical application prospects. Future research should focus on further validating the therapeutic effects and safety of YQJD in a broader population, especially through multicenter, randomized, controlled clinical trials. Moreover, studies should account for diverse patient populations (such as different ages and varying underlying conditions) to ensure the broad applicability of YQJD and optimal dosage adjustments.

While this study yielded promising results, several limitations remain. The use of Balb/c mice and HCECs as models, though widely applied in HSV-1 and keratitis research, may limit clinical translation due to species-specific immune differences and the lack of a complete *in vivo* environment. Future studies should incorporate diverse experimental models or preclinical research to further validate the safety and efficacy of YQJD, enhancing clinical relevance. Additionally, larger sample sizes, rigorous experimental designs, and exploration of unknown active compounds within YQJD are needed to fully assess its therapeutic potential for HSK.

In summary, this study confirms that the YQJD formula significantly inhibits HSV-1 infection-induced keratitis inflammation by modulating the expression of IL-4 and IL-6 and activating the PI3K/Akt signaling pathway, laying an experimental foundation for novel therapeutic strategies for HSK. These findings underscore the potential application of TCM formulas in modern medicine and pave the way for further clinical research and development. Despite the limitations, the results of this study offer a fresh perspective and foundation for future research in related fields, particularly in developing novel treatments targeting HSV-1 infection.

5. Conclusion

This study utilized UPLC-Q-Orbitrap HRMS to successfully identify 34 active components in the YQJD formula, including citric acid, caffeic acid, and uridine. Among them, Isovitexin and Formononetin exhibited the highest oral bioavailability. Through network pharmacology methods, 97 key targets for HSK treatment using the YQJD formula were screened, mainly involving anti-inflammatory and PI3K/Akt signaling pathways. Animal experiment results demonstrated that the YQJD formula alleviated corneal lesions in HSK mice and modulated the expression levels of inflammatory factors (IL-4, IL-6) and molecules related to the PI3K/Akt signaling pathway. Furthermore, cell experiments further confirmed that serum containing the YQJD formula regulated the expression of IL-4 in HCECs after HSV-1 infection. In conclusion, this study provides new theoretical foundations and molecular targets (Fig. 9) for treating HSK with the YQJD formula.

Ethics statement

All animal experiments were conducted in accordance with ethical guidelines and approved by the Animal Ethics Committee of Shuguang Hospital Affiliated to Shanghai University of Traditional Chinese Medicine (Approval No. PZSHUTCM180222039). The study adhered to the principles outlined in the Declaration of Helsinki and international ethical guidelines for animal research.

Funding

This project was supported by the Young Scientists Fund of the National Natural Science Foundation of China (81704124, 82104636).

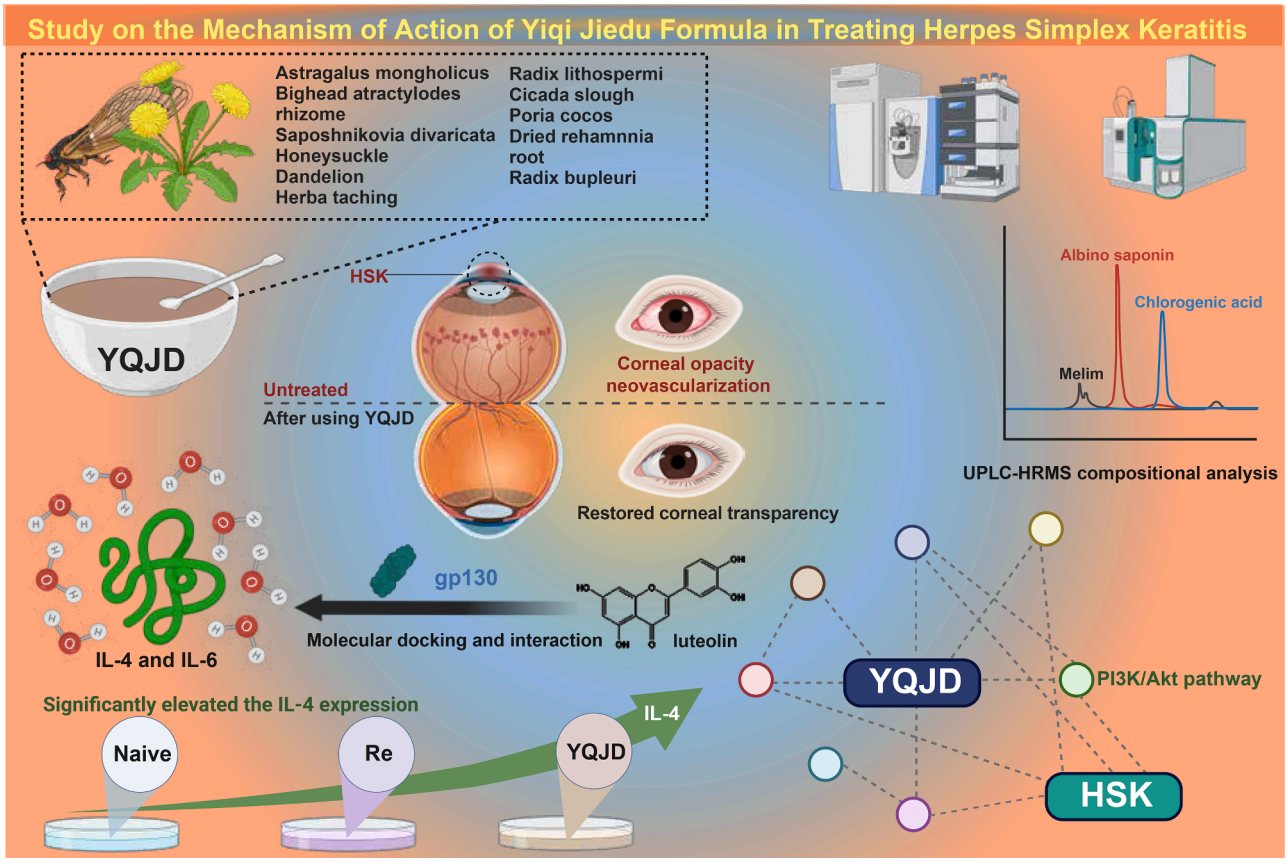

Fig. 9. Study on the mechanism of action of YQJD formula in treating HSK.

CRediT authorship contribution statement

Shuyu Xiao: Writing – review & editing, Writing – original draft, Visualization, Supervision, Resources, Methodology, Investigation, Data curation, Conceptualization. **Wanhong Miao:** Writing – original draft, Supervision, Methodology, Investigation, Formal analysis, Conceptualization. **Leilei Wang:** Writing – review & editing, Writing – original draft, Visualization, Supervision, Resources, Investigation, Data curation. **Lei Wang:** Writing – original draft, Software, Resources, Investigation, Data curation. **Sisi Tang:** Writing – original draft, Visualization, Validation, Methodology, Formal analysis. **Huihui Xu:** Visualization, Supervision, Resources, Investigation, Data curation. **Ying Yu:** Writing – review & editing, Writing – original draft, Validation, Project administration, Funding acquisition, Conceptualization.

Declaration of competing interest

The authors declare that they have no known competing financial interests or personal relationships that could have appeared to influence the work reported in this paper.

Acknowledgment

None.

Supplementary materials

Supplementary material associated with this article can be found, in the online version, at doi:10.1016/j.virusres.2025.199561.

Data availability

Data will be made available on request.

References

Almeida, I., Dias, L., Jesus, J., Fonseca, I., Matias, M.J., Pedro, J.C., 2022. Optical coherence tomography angiography in herpetic leucoma. BMC Med. Imaging. https://doi.org/10.1186/s12880-022-00747-z.

Barzegar Behrooz, A., Talaie, Z., Jusheghani, F., Łos, M.J., Klonisch, T., Ghavami, S., 2022. Wnt and PI3K/Akt/mTOR survival pathways as therapeutic targets in glioblastoma. IJMS. https://doi.org/10.3390/ijms23031353.

Bryant, A.E., Stevens, D.L., 2022. Investigating the immunomodulatory activities of omadacycline. J. Antimicrob. Chemother. https://doi.org/10.1093/jac/dkac356.

Chen, Y., Dong, J., Liu, J., Xu, W., Wei, Z., Li, Y., Wu, H., Xiao, H., 2019. Network pharmacology-based investigation of protective mechanism of aster tataricus on lipopolysaccharide-induced acute lung injury. IJMS. https://doi.org/10.3390/ijms20030543.

Chou, W.C., Rampanelli, E., Li, X., Ting, J.P.Y., 2021. Impact of intracellular innate immune receptors on immunometabolism. Cell Mol. Immunol. https://doi.org/10.1038/s41423-021-00780-y.

Danastas, K., Guo, G., Merjane, J., Hong, N., Larsen, A., Miranda-Saksena, M., Cunningham, A.L., 2023. Interferon inhibits the release of herpes simplex virus-1 from the axons of sensory neurons. mBio. https://doi.org/10.1128/mbio.01818-23.

Du, A., Li, S., Zhou, Y., Disoma, C., Liao, Y., Zhang, Y., Chen, Z., Yang, Q., Liu, P., Liu, S., Dong, Z., Razzaq, A., Tao, S., Chen, X., Liu, Y., Xu, L., Zhang, Q., Li, Shanni, Peng, J., Xia, Z., 2022. M6A-mediated upregulation of circMDK promotes tumorigenesis and acts as a nanotherapeutic target in hepatocellular carcinoma. Mol. Cancer. https://doi.org/10.1186/s12943-022-01575-z.

Efferth, T., Oesch, F., 2021. The immunosuppressive activity of artemisinin-type drugs towards inflammatory and autoimmune diseases. Med. Res. Rev. https://doi.org/10.1002/med.21842.

Feld, J.J., Lok, A.S., Zoulim, F., 2023. New perspectives on development of curative strategies for chronic hepatitis B. Clin. Gastroenterol. Hepatol. https://doi.org/10.1016/j.cgh.2023.02.032.

Haghighi-Najafabadi, N., Roohvand, F., Shams Nosrati, M.S., Teimoori-Toolabi, L., Azadmanesh, K., 2021. Oncolytic herpes simplex virus type-1 expressing IL-12 efficiently replicates and kills human colorectal cancer cells. Microb. Pathog. https://doi.org/10.1016/j.micpath.2021.105164.

Hinojosa, O.A., Ammari, O., 2023. Herpes simplex virus-associated aplastic anemia. Cureus. https://doi.org/10.7759/cureus.35320.

Hsin, K.Y., Ghosh, S., Kitano, H., 2013. Combining machine learning systems and multiple docking simulation packages to improve docking prediction reliability for network pharmacology. PLoS One. https://doi.org/10.1371/journal.pone.0083922.

Hu, Q., Zhang, W., Wu, Z., Tian, X., Xiang, J., Li, L., Li, Z., Peng, X., Wei, S., Ma, X., Zhao, Y., 2021. Baicalin and the liver-gut system: pharmacological bases explaining its therapeutic effects. Pharmacol. Res. https://doi.org/10.1016/j.phrs.2021.105444.

Huang, S., Hu, H., Tang, G., Liu, K., Luo, Z., Zeng, W., 2023. An oncolytic herpes simplex virus type 1 strain expressing a single-chain variable region antibody fragment against PD-1 and a PI3K inhibitor synergize to elicit antitumor immunity in ovarian cancer. Arch. Virol. https://doi.org/10.1007/s00705-023-05754-1.

Jaggi, U., Matundan, H.H., Lee, D.H., Ghiasi, H., 2022. Blocking autophagy in M1 macrophages enhances virus replication and eye disease in ocularly infected transgenic mice. J. Virol. https://doi.org/10.1128/jvi.01401-22.

Jiang, K., Feng, J., Qi, X., Ran, L., Xie, L., 2022. Antiviral activity of oridonin against herpes simplex virus type 1. DDDT. https://doi.org/10.2147/dddt.s387885.

Johnston, C., Magaret, A., Son, H., Stern, M., Rathbun, M., Renner, D., Szpara, M., Gunby, S., Ott, M., Jing, L., Campbell, V.L., Huang, M., Selke, S., Jerome, K.R., Koelle, D.M., Wald, A., 2022. Viral shedding 1 year following first-episode genital HSV-1 infection. JAMA. https://doi.org/10.1001/jama.2022.19061.

Kuzumi, A., Yoshizaki, A., Matsuda, K.M., Kotani, H., Norimatsu, Y., Fukayama, M., Ebata, S., Fukasawa, T., Yoshizaki-Ogawa, A., Asano, Y., Morikawa, K., Kazoe, Y., Mawatari, K., Kitamori, T., Sato, S., 2021. Interleukin-31 promotes fibrosis and T helper 2 polarization in systemic sclerosis. Nat. Commun. https://doi.org/10.1038/s41467-021-26099-w.

Li Puma, D.D., Colussi, C., Bandiera, B., Puliatti, G., Rinaudo, M., Cocco, S., Paciello, F., Re, A., Ripoli, C., De Chiara, G., Bertozzi, A., Palamara, A.T., Piacentini, R., Grassi, C., 2023. Interleukin 1β triggers synaptic and memory deficits in Herpes simplex virus type-1-infected mice by downregulating the expression of synaptic plasticity-related genes via the epigenetic MeCP2/HDAC4 complex. Cell Mol. Life Sci. https://doi.org/10.1007/s00018-023-04817-5.

Li, W., Xu, C., Hao, C., Zhang, Y., Wang, Z., Wang, S., Wang, W., 2020. Inhibition of herpes simplex virus by myricetin through targeting viral gD protein and cellular EGFR/PI3K/Akt pathway. Antivir. Res. https://doi.org/10.1016/j.antiviral.2020.104714.

Li, Z., Lai, X., Fu, S., Ren, L., Cai, H., Zhang, H., Gu, Z., Ma, X., Luo, K., 2022. Immunogenic cell death activates the tumor immune microenvironment to boost the immunotherapy efficiency. Adv. Sci. https://doi.org/10.1002/advs.202201734.

Lomenick, B., Hao, R., Jonai, N., Chin, R.M., Aghajan, M., Warburton, S., Wang, J., Wu, R.P., Gomez, F., Loo, J.A., Wohlschlegel, J.A., Vondriska, T.M., Pelletier, J., Herschman, H.R., Clardy, J., Clarke, C.F., Huang, J., 2009. Target identification using drug affinity responsive target stability (DARTS). Proc. Natl. Acad. Sci. U. S. A. https://doi.org/10.1073/pnas.0910040106.

Long, H.Z., Cheng, Y., Zhou, Z.W., Luo, H.Y., Wen, D.D., Gao, L.C., 2021. PI3K/AKT signal pathway: a target of natural products in the prevention and treatment of Alzheimer's disease and Parkinson's disease. Front. Pharmacol. https://doi.org/10.3389/fphar.2021.648636.

Lu, D., Yang, Y., Du, Y., Zhang, L., Yang, Yi, Tibenda, J.J., Nan, Y., Yuan, L., 2023. The potential of glycyrrhiza from "Medicine food homology" in the fight against digestive system tumors. Molecules. https://doi.org/10.3390/molecules28237719.

Luan, D., Dadpey, B., Zaid, J., Bridge-Comer, P.E., DeLuca, J.H., Xia, W., Castle, J., Reilly, S.M., 2022. Adipocyte-secreted IL-6 sensitizes macrophages to IL-4 signaling. Diabetes. https://doi.org/10.2337/db22-0444.

Masuda, T., Ino, Y., Hirai, A., Okamura, A., Ishikawa, H., Yokoyama, S., Osawa, T., 2021. Effects of isoflavone-rich red clover extract on blood glucose level: a randomized, double-blind, placebo-controlled trial. J. Food Sci. https://doi.org/10.1111/1750-3841.15672.

McCarthy, M.W., 2022. Ensitrelvir as a potential treatment for COVID-19. Expert Opin. Pharmacother. https://doi.org/10.1080/14656566.2022.2146493.

Möckel, M., De La Cruz, N.C., Rübsam, M., Wirtz, L., Tantcheva-Poor, I., Malter, W., Zinser, M., Bieber, T., Knebel-Mörsdorf, D., 2022. Herpes simplex virus 1 can bypass impaired epidermal barriers upon *ex vivo* infection of skin from atopic dermatitis patients. J. Virol. https://doi.org/10.1128/jvi.00864-22.

Morris, J., Stuart, P.M., Rogge, M., Potter, C., Gupta, N., Yin, X.T., 2012. Recurrent herpetic stromal keratitis in mice, a model for studying human HSK. JoVE. https://doi.org/10.3791/4276.

Mustafa, S., Riaz, M.A., Masoud, M.S., Qasim, M., Riaz, A., 2022. Impact of dietary inclusion of Chenopodium quinoa on growth performance and survival of Hubbard chicken. PLoS One. https://doi.org/10.1371/journal.pone.0276524.

Naqvi, R.A., Valverde, A., Yadavalli, T., Bobat, F.I., Capistrano, K.J., Shukla, D., Naqvi, A. R., 2024. Viral MicroRNAs in herpes simplex virus 1 pathobiology. CPD. https://doi.org/10.2174/0113816128286469240129100313.

Naudhani, M., Thakur, K., Ni, Z.J., Zhang, J.G., Wei, Z.J., 2021. Formononetin reshapes the gut microbiota, prevents progression of obesity and improves host metabolism. Food Funct. https://doi.org/10.1039/d1fo02942h.

Oh, P.S., Han, Y.H., Lim, S., Jeong, H.J., 2023. Blue light irradiation exerts anti-viral and anti-inflammatory properties against herpes simplex virus type 1 infection. J. Photochem. Photobiol. B Biol. https://doi.org/10.1016/j.jphotobiol.2022.112632.

Parvez, S., Herdman, C., Beerens, M., Chakraborti, K., Harmer, Z.P., Yeh, J.R.J., MacRae, C.A., Yost, H.J., Peterson, R.T., 2021. MIC-Drop: a platform for large-scale *in vivo* CRISPR screens. Science. https://doi.org/10.1126/science.abi8870 (1979).

Qu, J., Li, J., Zhang, Y., He, R., Liu, X., Gong, K., Duan, L., Luo, W., Hu, Z., Wang, G., Xia, C., Luo, D., 2021. AKR1B10 promotes breast cancer cell proliferation and migration via the PI3K/AKT/NF-κB signaling pathway. Cell Biosci. https://doi.org/10.1186/s13578-021-00677-3.

Qu, J., Qiu, B., Zhang, Y., Hu, Y., Wang, Z., Guan, Z., Qin, Y., Sui, T., Wu, F., Li, B., Han, W., Peng, X., 2023. The tumor-enriched small molecule gambogic amide

suppresses glioma by targeting WDR1-dependent cytoskeleton remodeling. Sig Transduct. Target. Ther. https://doi.org/10.1038/s41392-023-01666-3.
Rathbun, M.M., Szpara, M.L., 2021. A holistic perspective on herpes simplex virus (HSV) ecology and evolution. Adv Virus Res. https://doi.org/10.1016/bs.aivir.2021.05.001.
Romo, M.L., Osorio, R., Toledo, A., Carrillo-Mezo, R., Valdez, R., Romano, M.C., Sciutto, E., Fragoso, G., Fleury, A., 2023. Low responsiveness of peripheral lymphocytes in extraparenchymal neurocysticercosis. PLoS Negl. Trop. Dis. https://doi.org/10.1371/journal.pntd.0011386.
Rousseau, A., Pharm, S.B., Gueudry, J., Deback, C., Haigh, O., Schweitzer, C., Boutolleau, D., Labetoulle, M., 2022. Acyclovir-resistant herpes simplex virus 1 keratitis: a concerning and emerging clinical challenge. Am. J. Ophthalmol. https://doi.org/10.1016/j.ajo.2022.01.010.
Scallan, J.P., Jannaway, M., 2022. Lymphatic vascular permeability. Cold Spring Harb. Perspect. Med. https://doi.org/10.1101/cshperspect.a041274.
Sendra, V.G., Tau, J., Zapata, G., Lasagni Vitar, R.M., Illian, E., Chiaradía, P., Berra, A., 2021. Polluted air exposure compromises corneal immunity and exacerbates inflammation in acute herpes simplex keratitis. Front. Immunol. https://doi.org/10.3389/fimmu.2021.618597.
Shah, A., Farooq, A.V., Tiwari, V., Kim, M.J., Shukla, D., 2010. HSV-1 infection of human corneal epithelial cells: receptor-mediated entry and trends of re-infection. Mol. Vis. 16, 2476–2486.
Shang, L., Wang, Y., Li, J., Zhou, F., Xiao, K., Liu, Y., Zhang, M., Wang, S., Yang, S., 2023. Mechanism of Sijunzi decoction in the treatment of colorectal cancer based on network pharmacology and experimental validation. J. Ethnopharmacol. https://doi.org/10.1016/j.jep.2022.115876.
Sun, E.J., Wankell, M., Palamuthusingam, P., McFarlane, C., Hebbard, L., 2021. Targeting the PI3K/Akt/mTOR pathway in hepatocellular carcinoma. Biomedicines. https://doi.org/10.3390/biomedicines9111639.
Tang, Y.P., Xu, D.Q., Yue, S.J., Chen, Y.Y., Fu, R.J., BAI, X., 2022. Modern research thoughts and methods on bio-active components of TCM formulae. Chin. J. Nat. Med. https://doi.org/10.1016/s1875-5364(22)60206-1.
Teede, H.J., McGrath, B.P., DeSilva, L., Cehun, M., Fassoulakis, A., Nestel, P.J., 2003. Isoflavones reduce arterial stiffness. ATVB. https://doi.org/10.1161/01.atv.0000072967.97296.4a.
van Velzen, M., van de Vijver, D.A.M.C., van Loenen, F.B., Osterhaus, A.D.M.E., Remeijer, L., Verjans, G.M.G.M., 2013. Acyclovir prophylaxis predisposes to antiviral-resistant recurrent herpetic keratitis. J. Infect. Dis. https://doi.org/10.1093/infdis/jit350.
Van Wagoner, N., Qushair, F., Johnston, C., 2023. Genital herpes infection. Infect. Dis. Clin. N. Am. https://doi.org/10.1016/j.idc.2023.02.011.
Wang, Yuan, Li, F., Wang, Z., Song, X., Ren, Z., Wang, X., Wang, Yifei, Zheng, K., 2023. Luteolin inhibits herpes simplex virus 1 infection by activating cyclic guanosine monophosphate-adenosine monophosphate synthase-mediated antiviral innate immunity. Phytomedicine. https://doi.org/10.1016/j.phymed.2023.155020.
Wei, W., Mu, S., Han, Y., Chen, Y., Kuang, Z., Wu, X., Luo, Y., Tong, C., Zhang, Y., Yang, Y., Song, Z., 2022. Gpr174 knockout alleviates DSS-induced colitis via regulating the immune function of dendritic cells. Front. Immunol. https://doi.org/10.3389/fimmu.2022.841254.
Xiao, S., Yang, Y., Miao, W., Lyu, C., Tao, J., Yu, Y., 2022. Activation of the STAT5 signaling pathway by Yiqi Jiedu formula induces regulatory T cell-mediated alleviation of corneal immunopathological damage in mice with recurrent herpes simplex keratitis. Front. Pharmacol. https://doi.org/10.3389/fphar.2021.790787.
Xue, L., Jin, X., Ji, T., Li, R., Zhuge, X., Xu, F., Quan, Z., Tong, H., Yu, W., 2023. Luteolin ameliorates DSS-induced colitis in mice via suppressing macrophage activation and chemotaxis. Int. Immunopharmacol. https://doi.org/10.1016/j.intimp.2023.110996.
Yin, Y., Wang, Y., Wang, C., Zhang, Y., Qi, A., Song, J., Xu, L., Yang, W., Jiao, L., 2024. Predicting the mechanism of action of YQYYJD prescription in the treatment of non-small cell lung cancer using transcriptomics analysis. J. Ethnopharmacol. https://doi.org/10.1016/j.jep.2024.117984.
Zhang, Q., Wang, L., Wang, S., Cheng, H., Xu, L., Pei, G., Wang, Y., Fu, C., Jiang, Y., He, C., Wei, Q., 2022. Signaling pathways and targeted therapy for myocardial infarction. Signal Transduct. Target. Ther. https://doi.org/10.1038/s41392-022-00925-z.
Zhang, X., Chen, X., Wang, L., Wang, A., He, C., Shi, Z., Zhang, S., Fu, Q., Xu, W., Hu, S., 2022. Protective effects of Yiqi jiedu decoction on ionizing radiation-induced spermatogenic cell injury. J. Ethnopharmacol. https://doi.org/10.1016/j.jep.2022.115681.
Zhao, L., Zhang, H., Li, N., Chen, J., Xu, H., Wang, Y., Liang, Q., 2023. Network pharmacology, a promising approach to reveal the pharmacology mechanism of Chinese medicine formula. J. Ethnopharmacol. https://doi.org/10.1016/j.jep.2023.116306.
Zhao, Y., Zhang, W., Huo, M., Wang, P., Liu, X., Wang, Y., Li, Y., Zhou, Z., Xu, N., Zhu, H., 2021. XBP1 regulates the protumoral function of tumor-associated macrophages in human colorectal cancer. Signal Transduct. Target. Ther. https://doi.org/10.1038/s41392-021-00761-7.
Zheng, S., Xue, T., Wang, B., Guo, H., Liu, Q., 2022. Chinese medicine in the treatment of ulcerative colitis: the mechanisms of signaling pathway regulations. Am. J. Chin. Med. https://doi.org/10.1142/s0192415x22500756.
Zhou, F., Wang, W., Xu, R., Liu, L., Lin, T., He, L., Tang, L., Wang, X., He, Y., 2024. Unraveling the mechanism of Yiqi Jiedu formula against nasopharyngeal carcinoma: an investigation integrating network pharmacology, serum pharmacochemistry, and metabolomics. J. Ethnopharmacol. https://doi.org/10.1016/j.jep.2023.117343.
Zhou, J.Y., Wu, C., Shen, Z., Liu, S., Zou, X., Qian, J., Wu, Z., Huan, X., Mu, B.X., Ye, N., Ning, Y., Wang, Y., Chen, M., Zhuang, Y., 2024. Yiqi Huayu Jiedu Decoction inhibits liver metastasis of colorectal cancer via enhancing natural killer cells function. J. Ethnopharmacol. https://doi.org/10.1016/j.jep.2023.116915.
Zhu, J.Y., Zhang, X., Zheng, X., Luo, L.L., Mao, C.Y., Lin, S., Ye, J., 2022. Dry eye symptoms in interferon regulatory factor 3-deficient mice due to herpes simplex virus infection in Harderian gland and lacrimal gland. Exp. Eye Res. https://doi.org/10.1016/j.exer.2022.109053.